HHS Public Access

Author manuscript

Cell Rep. Author manuscript; available in PMC 2020 May 10.

Published in final edited form as:

Cell Rep. 2020 April 14; 31(2): 107496. doi:10.1016/j.celrep.2020.03.060.

Progesterone Receptor Serves the Ovary as a Trigger of Ovulation and a Terminator of Inflammation

Chan Jin Park[1], **Po-Ching Lin**[1], **Sherry Zhou**[1], **Radwa Barakat**[1,2], **Shah Tauseef Bashir**[1], **Jeong Moon Choi**[1], **Joseph A. Cacioppo**[1], **Oliver R. Oakley**[3], **Diane M. Duffy**[4], **John P. Lydon**[5], **CheMyong J. Ko**[1,6,*]

[1]Department of Comparative Biosciences, College of Veterinary Medicine, University of Illinois at Urbana-Champaign, 2001 South Lincoln Avenue, Urbana, IL 61802, USA

[2]Department of Toxicology and Forensic Medicine, College of Veterinary Medicine, Benha University, Qalyubia 13518, Egypt

[3]Department of Biological Sciences, Eastern Kentucky University, Richmond, KY 40475, USA

[4]Department of Physiological Sciences, Eastern Virginia Medical School, PO Box 1980, Norfolk, VA 23501, USA

[5]Department of Molecular and Cellular Biology, Baylor College of Medicine, Houston, TX 77030, USA

[6]Lead Contact

SUMMARY

Ovulation is triggered by the gonadotropin surge that induces the expression of two key genes, progesterone receptor (*Pgr*) and prostaglandin-endoperoxide synthase 2 (*Ptgs2*), in the granulosa cells of preovulatory follicles. Their gene products PGR and PTGS2 activate two separate pathways that are both essential for successful ovulation. Here, we show that the PGR plays an additional essential role: it attenuates ovulatory inflammation by diminishing the gonadotropin surge-induced *Ptgs2* expression. PGR indirectly terminates *Ptgs2* expression and PGE2 synthesis in granulosa cells by inhibiting the nuclear factor κB (NF-κB), a transcription factor required for *Ptgs2* expression. When the expression of PGR is ablated in granulosa cells, the ovary undergoes a hyperinflammatory condition manifested by excessive PGE2 synthesis, immune cell infiltration, oxidative damage, and neoplastic transformation of ovarian cells. The PGR-driven termination of PTGS2 expression may protect the ovary from ovulatory inflammation.

*Correspondence: jayko@illinois.edu.

AUTHOR CONTRIBUTIONS

C.J.P. and C.J.K. designed and performed experiments, analyzed and interpreted data, and wrote the manuscript. P.-C.L., S.Z., and J.M.C. designed and performed experiments and analyzed data. R.B., S.T.B., J.A.C., and O.R.O. designed experiments and interpreted data. J.P.L. provided critical transgenic mice. D.M.D. interpreted data and edited the manuscript. All authors edited and approved the final manuscript.

SUPPLEMENTAL INFORMATION

Supplemental Information can be found online at https://doi.org/10.1016/j.celrep.2020.03.060.

DECLARATION OF INTERESTS

The authors declare no competing interests.

Graphical Abstract

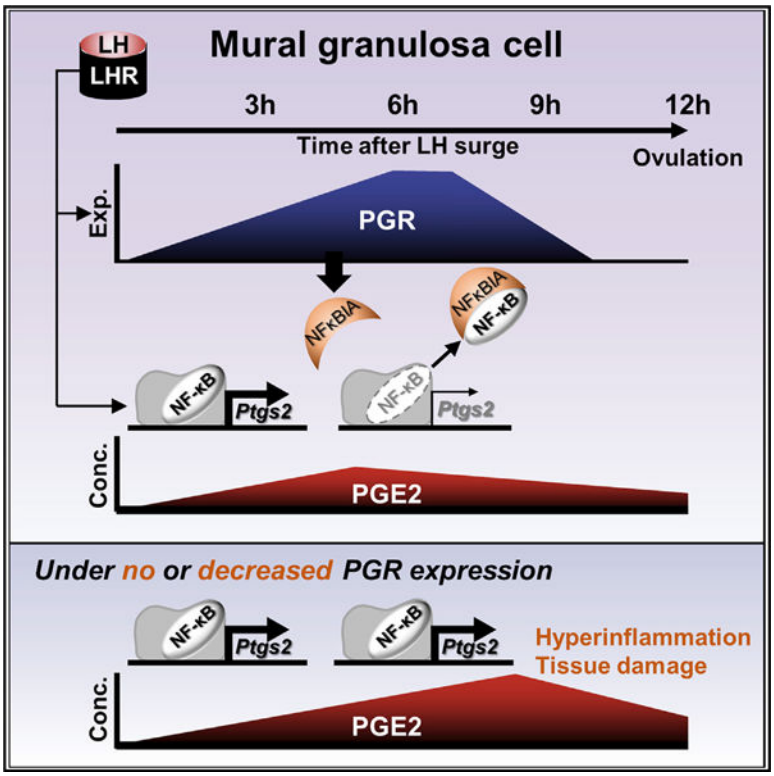

In Brief

A preovulatory LH surge induces the expression of PGR and the production of PGE2, a proinflammatory prostaglandin, in preovulatory granulosa cells. Park et al. show that PGR then suppresses PGE2 synthesis by decreasing the expression of PTGS2. Such PGR-driven termination temporarily confines ovulatory inflammation within a short period.

INTRODUCTION

In most mammalian species, a female ovulates multiple times in her lifetime. In humans, a typical woman will undergo >360 ovulations before reaching menopause (one ovulation/month × 30 years = 360). Each ovulation is accompanied by acute inflammatory events that are driven by prostaglandin-endoperoxide synthase 2 (PTGS2; also known as COX-2) expression (Duffy et al., 2019; Jabbour et al., 2009; Richards et al., 2002; Spanel-Borowski, 2011) and also by a physical tear of the ovarian tissue at the site of oocyte release. PTGS2 is a rate-limiting enzyme in prostaglandin E2 (PGE2) synthesis (DeWitt, 1991; Needleman et al., 1986). Mice deficient in *Ptgs2* expression fail to ovulate (Davis et al., 1999). In the ovary, PGE2 regulates angiogenesis, blood flow, immune cell function, and tissue remodeling associated with cumulus expansion, follicle wall proteolysis, and formation of the corpus luteum (Duffy et al., 2019). Importantly, PGE2 is an inflammatory prostaglandin that, in concert with pro-inflammatory cytokines, induces inflammation in the ovulating ovary (Espey, 1980, 1994; Jabbour et al., 2009; Richards et al., 2002; Sirois et al., 2004;

Spanel-Borowski, 2011). Locally produced PGE2 stimulates the recruitment of immune cells, including but not limited to dendritic cells, monocytes, and neutrophils to the ovary (Jabbour et al., 2009), similar to its function in other inflammatory sites (Ricciotti and FitzGerald, 2011). We previously demonstrated that the ovulatory gonadotropin surge immediately increases leukocyte population sizes in the ovary (Oakley et al., 2010, 2011).

The leukocyte recruitment is triggered by pro-inflammatory cytokines and reactive oxygen species (ROS) that are either released by ovarian stroma cells or resident leukocytes (Espey, 1980; Jablonka-Shariff and Olson, 1998; Kodaman and Behrman, 2001; Ness and Cottreau, 1999; Shukovski and Tsafriri, 1994; Yamauchi et al., 1997). Ovulation itself cause the DNA damage and pathological change in the ovary (Jia et al., 2018; Murdoch et al., 2001; Savant et al., 2018; Yang-Hartwich et al., 2014). Hence, repeated ovulations likely accumulate such damages in the ovary (Spanel-Borowski, 2011), which may become manifested later in life. Indeed, women who take a contraceptive pill to prevent ovulation has a lower probability to develop ovarian cancer than those who do not (Iversen et al., 2018). Furthermore, aberrant inflammation alters normal ovarian follicular dynamics, resulting in impaired oocyte quality, anovulation, and associated infertility (Boots and Jungheim, 2015). Nonetheless, the ovary that undergoes repetitive ovulations still maintains its structural and functional integrity for decades, indicating an existence of a mechanism that protects the ovarian tissue from the repetitive ovulatory inflammations and/or confines the ovulatory inflammation either temporally, spatially, or both, and thereby minimizes tissue damage. If the inflammation is not properly controlled, damage to the ovary may be exacerbated by each ovulatory inflammation, leading to the premature loss of its structural integrity and function. Presently, it is not known how the ovary protects itself from repeated ovulatory inflammations.

Ovulation is an event that involves multiple hormone-receptor interactions, cell proliferation and differentiation, specifically timed gene expressions, inflammatory processes, and tissue remodeling. These events are triggered by a preovulatory surge of luteinizing hormone (LH) (Peng et al., 1991; Richards and Ascoli, 2018; Richards et al., 1998; Robker and Richards, 1998) that concurrently induces the expression of two key ovulation genes, progesterone receptor (*Pgr*) and *Ptgs2*, specifically in the granulosa cells of preovulatory follicles (Morris and Richards, 1995; Natraj and Richards, 1993; Park and Mayo, 1991; Sirois et al., 1992, 1993). *Pgr* encodes the nuclear receptor transcription factor PGR, which plays critical roles in regulating reproduction at all levels of the hypothalamus-pituitary-ovary axis (Chappell et al., 1997, 1999; Gal et al., 2016; White et al., 2007) as demonstrated by the loss of fertility when a null mutation is introduced in the *Pgr* gene (Kubota et al., 2016; Lydon et al., 1995). PTGS2 plays a critical role in ovulation by promoting PGE2 synthesis and driving ovulatory inflammation, as described above.

The simultaneous induction of PGR and PTGS2 expression in the same cell (preovulatory granulosa cells) by a single signal, LH, is an intriguing phenomenon. Generally, these two proteins drive functionally opposing physiological events: PTGS2 expression promotes inflammation by producing pro-inflammatory prostaglandins (Ricciotti and FitzGerald, 2011), whereas PGR acts as an anti-inflammatory mediator by either inducing the expression of anti-inflammatory genes or suppressing the expression of pro-inflammatory genes (Renthal et al., 2013; Wei and Xiao, 2013). Why are these two functionally opposing

proteins simultaneously induced by a single trigger? In this study, we aimed to investigate the physiological significance of this phenomenon under the hypothesis that PGR stimulates the cascade of pro-ovulatory events (Akison and Robker, 2012; Kim et al., 2009) but also attenuates ovulatory inflammation by terminating LH-induced PTGS2 expression, thereby minimizing tissue damage in the ovary. A mutant mouse strain that is selectively deficient of *Pgr* gene in the granulosa cells was created and used as an animal model for testing the hypothesis at the physiological level, and a single-cell RNA sequencing (RNA-seq) approach and molecular tools were used to identify the action mechanism of PGR in regulating *Ptgs2* expression. This study demonstrates the critical role that PGR plays in the granulosa cells for successful ovulation and reports a role of PGR as a silencer of *Ptgs2* expression in the granulosa cells of the preovulatory ovary.

RESULTS

Loss of PGR Expression in the Granulosa Cell Results in Ovulatory Failure

The functional role of PGR in the granulosa cells of preovulatory follicle was assessed by creating a mouse strain in which *Pgr* expression was ablated selectively in the granulosa cells. This strain was generated by cross-breeding floxed *Pgr* mice with *Esr2*^{iCre} mice that, in the ovary, express Cre recombinase exclusively in the granulosa cells (Figure 1A; Figure S1; Cacioppo et al., 2016). Ablation of PGR expression in this mutant line (*Pgr*$^{flox/flox}$*Esr2*$^{iCre/wt}$; Esr2-PgrKO) was confirmed by RT-PCR, western blot, and immunohistochemistry (Figures 1B–1D). In the wild-type (WT) ovary, PGR expression is induced in the granulosa cells of large antral follicles and interstitial cells 6 h after ovulatory gonadotropin (hCG) stimulation. In the Esr2-Pgr knockout (KO) mouse, PGR expression was ablated selectively in the granulosa cells of large antral follicles, whereas the expression was maintained in the interstitium (Figure 1D).

Esr2-PgrKO mice did not ovulate upon ovulatory gonadotropin stimulation (Figures 1E and F). Instead, entrapped oocytes were present inside corpora lutea (CL) 20 h after hCG stimulation, indicating CL formation without ovulation (Figure 1G). In general, the phenotypes of CL with entrapped oocytes did not differ between Esr2-PgrKO and PgrKO (global *Pgr* KO) ovaries (Figure 1H). Not surprisingly, Esr2-PgrKO female mice were completely infertile; no breeding trial resulted in a birth (Figure 1I). However, unlike PgrKO mice that do not cycle (Kubota et al., 2016; Lydon et al., 1995), vaginal cytology revealed that Esr2-PgrKO mice exhibited a pattern of estrous cycles that is comparable to those of WT mice (Figure 1J), indicating that they retain a functioning PGR in the hypothalamus-pituitary axis and normal cyclic synthesis of ovarian steroids, estradiol, and progesterone in the ovary (Kubota et al., 2016).

Elevated *Ptgs2* Expression in Esr2-PgrKO Granulosa Cells

PGR regulates a cohort of key ovulatory genes in granulosa cells (Duffy et al., 2019; Kim et al., 2009; Richards, 2018; Sriraman et al., 2010). RT-PCR assays indeed showed that, upon gonadotropin stimulation, the expression levels of known PGR-downstream genes, such as a disintegrin and metalloproteinase with thrombospondin motifs 1 (*Adamts-1*) (Robker et al., 2000), chemokine receptor 4 (*Cxcr4*) (Choi et al., 2017), synaptosomal-associated protein 25

(*Snap25*) (Shimada et al., 2007), and fatty acid binding protein 4 (*Fabp4*) (Sriraman et al., 2010), were significantly lower in the granulosa cells of Esr2-PgrKO than those of WT (Figure S2A).

To further look into the effect of PGR ablation in granulosa cells at the individual ovarian cell level, WT and Esr2-PgrKO ovaries were collected 6 h after hCG injection, and their transcriptomes were compared by single-cell RNA-seq. For each genotype, dissociated ovarian cells from 4 mice were pooled. Among them, we randomly isolated 3,200 cells (representing approximately 0.6% of total cells in an ovary), and their transcriptomes were examined by RNA-seq. As expected, read count of the transcripts from exon 2 of the *Pgr* gene, the floxed exon, was markedly decreased in the granulosa cells of Esr2-PgrKO compared to those of WT, indicating successful deletion of the exon 2 (Figure S2B). Profiling of gene expression patterns at individual cell levels by using the Uniform Manifold Approximation and Projection (UMAP) led us to group the total ovarian cells into 18 clusters of cell types (0–17) (Figure 2A). By using established marker genes of ovarian cells, we identified some of the clusters as early-stage granulosa cells (Early-GC) that were from immature follicles, mural granulosa cells from ovulatory follicles (Ov-mural-1 and −2), cumulus cells from ovulatory follicles (Ov-cumulus), theca cells, endothelial cells, interstitial cells, and immune cells (Figure S3A), but the identities of some clusters were not known (Figure 2A). Granulosa cells accounted for 62% of the total cells. In each sub-cluster of granulosa cells, different numbers and sets of genes were affected by the PGR ablation. For example, Ov-mural-1, Ov-mural-2, and Ov-cumulus clusters of cells had 667 (643, adjusted [adj] $p < 0.05$), 248 (184, adj $p < 0.05$), and 355 (314, adj $p < 0.05$) genes that were differentially expressed between WT and Esr2-PgrKO, respectively (Figure S3B; Table S1). Notably, 414 differentially expressed genes (log fold change [FC] < -0.25 or > 0.25, but not significant) were found in the immune cluster (Figure 2B; Table S1), whereas fewer genes showed altered expression in other cell clusters (Figure S3C).

Interestingly, expression of the *Ptgs2* gene was upregulated only in the ovulatory mural granulosa cells of Esr2-PgrKO compared to those of WT (logFC 1.283, 0.917, and 1.070 in Ov-mural-1, OV-mural-2, and Ov-cumulus, respectively; adj $p < 0.05$) but not in cells of other clusters. The violin plot also showed that the *Ptgs2* expression level was markedly higher in the clusters 0 (Ov-mural-1), 3 (Ov-cumulus), and 4 (Ov-mural-2) of Esr2-PgrKO than those of WT clusters (Figure 2C; Table S1). Notably, the expression of *S100a6*, a known PGR-downstream gene, was lower in those granulosa cell clusters of the Esr2-PgrKO ovary (Figure 2C). Intriguingly, UMAP clustering showed that *Ptgs2* expression was elevated specifically in the granulosa cells that were to express *Pgr* (Figure 2D), indicating a negative correlation between *Pgr* and *Ptgs2* expression in the granulosa cells.

PGR Downregulates *Ptgs2* Expression in the Granulosa Cells

Spatiotemporal patterns of PTGS2 and PGR protein expression were measured at 0, 3, 6, 9, and 12 h after hCG stimulation by immunohistochemistry assay (Figure S4A). At 3 h post-hCG injection, expression of both PGR and PTGS2 was induced in the mural granulosa cells. In the cumulus granulosa cells, however, only PTGS2 but not PGR was expressed (Figure S4A). This pattern was not different at hCG 6 h, where PGR expression was seen

only in mural granulosa cells, whereas PTGS2 was localized in both mural granulosa and cumulus cells. At hCG 9 and 12 h, PTGS2 expression was decreased in the mural granulosa cells but not in the cumulus cells (Figure S4A).

The functional significance of the unique expression patterns between PGR and PTGS2 was then sought using the singlecell RNA-seq data (Figure 2). Using UMAP clustering, we virtually isolated mural granulosa cells (*Ube2c*-negative) and used them for t-distributed stochastic neighbor embedding (t-SNE) clustering and cell trajectory prediction (Figure 3A). The Pseudotime cell trajectory predicted by Monocle 2 (Trapnell et al., 2014) identified two different sub-groups (ovulatory and non-ovulatory branches) of granulosa cells (Figure 3B). *Pgr* and its known downstream gene *Snap25* were predominantly expressed in Branch-1 of WT cells. As expected, Branch-1 of Esr2-PgrKO cells did not express *Snap25*. Importantly, the *Ptgs2* gene began to express at about the same time in the WT and Esr2-PgrKO granulosa cells. Interestingly, however, the *Ptgs2* expression level gradually decreased when *Pgr* expression increased in WT mural granulosa cells. In Esr2-PgrKO granulosa cells, *Ptgs2* expression remained high during the same period. Meanwhile, cells in Branch-1 had a low expression level of *Amh* throughout the entire cell trajectory, whereas Branch-2 maintained a relatively higher *Amh* level (Figure 3B). Interestingly, we found that the gene *Lyve1* was highly expressed in Branch-1 of WT granulosa cells toward the end of granulosa cell differentiation but not at all in Esr2-PgrKO cells, indicating that this is a PGR downstream gene (Figure 3B). Indeed, immunohistochemistry showed that LYVE1 expression was induced upon stimulation by gonadotropin in the WT granulosa cells but not in the Esr2-PgrKO cells (Figure S4B). LYVE1 is known to play a role in transporting hyaluronan in the lymphatic endothelial cells (Johnson et al., 2007; Prevo et al., 2001).

To verify if *Ptgs2* expression was regulated by PGR, *Ptgs2*/PTGS2 expression patterns and PGE2 contents were compared in preovulatory follicles of WT and Esr2-PgrKO ovaries after stimulation by gonadotropin injection. Immune-localization of PTGS2, RT-PCR, and western blot assays showed that granulosa cells from Esr2-PgrKO ovaries had higher contents of *Ptgs2* mRNA and PTGS2 protein than those of WT (Figures 3C–3E). To determine if the increased *Ptgs2* expression led to an elevated PGE2 synthesis in the Esr2-PgrKO ovary, total ovarian PGE2 levels were measured during the period of the gonadotropin-induced ovulatory period. Ovaries were collected at 0, 6, 9, and 12 h after hCG stimulation, and their ovarian PGE2 contents were determined. Upon hCG injection, ovarian PGE2 contents rapidly increased, reaching the highest level at hCG 6 h. The level was maintained until hCG 9 h but returned to basal at hCG 12 h in the WT (Figure 3F). This temporal pattern is consistent with the temporal PTGS2 protein expression in the WT ovaries (Figure S4A). However, Esr2-PgrKO ovaries showed significantly higher ovarian PGE2 levels at hCG 6 h and 9 h than WT ovaries (Figure 3F), indicating that a PGR plays a negative regulatory role in PTGS2 expression and PGE2 synthesis.

The potential regulatory role of PGR on *Ptgs2* expression in granulosa cells was first explored using chromatin immunoprecipitation sequencing (ChIP-seq) data obtained from a public repository (GEO: GSE115820) (Dinh et al., 2019) in which the genome-wide PGR binding sites were reported in the granulosa cells. The ChIP-seq data analysis indicated a weak or no PGR binding to *Ptgs2* gene in the granulosa cells of hCG-stimulated granulosa

cells (Figure S5A) but did indicate a strong occupancy of PGR in the upstream region of *Nfkbia* (a gene encoding NF-κB inhibitor α [NFκBIA]) (Figure S5A). NF-κB acts as a key transcription factor that directly binds to the *Ptgs2* promoter and enhances its transcriptional activity (Klein et al., 2007; Yang and Bleich, 2004). When NF-κB is bound by NFκBIA, it loses its transcriptional activity (Zhang et al., 2017). Indeed, PGR is known to increase *Nfkbia* expression by directly binding to its promotor in uterine myometrial cells (Hardy et al., 2006; Mendelson, 2009). Therefore, we reasoned that PGR might attenuate *Ptgs2* expression by upregulating NFκBIA expression (Figure S5A). Single-cell RNA-seq data showed that expression levels of NF-κB subunits *Nfkb1* and *Rela* in mural granulosa cells were not different between WT and Esr2-PgrKO (Figure S5B). However, the *Nfkbia* expression level was lower in the Esr2-PgrKO mural granulosa cells than the WT (Figure 4A). A two-dimensional scatterplot analysis that was generated using *Ptgs2* and *Nfkbia* expression data obtained from ovulatory mural granulosa cells showed that WT and Esr2-PgrKO ovaries had more *Nfkbia*-positive cells and *Ptgs2*-positive cells, respectively, than the other genotype (Figure S5C). Indeed, *Nfκbia* expression was decreased in the Esr2-PgrKO (Figure 4B), whereas the level of acetyl-p65 protein, a subunit of the active form of NF-κB, was elevated in the Esr2-PgrKO granulosa cells (Figure 4C). In cultured granulosa cells, the *Nfkbia* expression level was increased by hCG treatment but decreased by treatment with RU486, a PGR antagonist, in cultured granulosa cells (Figure 4D). In these cells, *Ptgs2* mRNA was increased 4-fold upon hCG treatment alone and was increased by 8fold when additionally treated with progesterone and RU486. Immunoprecipitation using an anti-acetyl p65 in the granulosa cells that were treated with hCG and RU486 followed by PCR amplification of the chromatin showed that the binding of acetyl-p65 to the proximal promoter (−401/−393 and —93/−88) of the *Ptgs2* gene increased when the granulosa cells were treated with RU486 (Figure 4E), supporting the idea that PGR inhibits *Ptgs2* expression by regulating NF-κB activity by increasing NFκBIA expression.

Loss of PGR Expression Causes Excessive Immune Cell Influx to the Ovary

Excessive or uncontrolled PGE2 synthesis during ovulation may cause a hyper-inflammation, leading to inflammatory damage to the ovary (Jabbour et al., 2009; Kidane et al., 2014). Therefore, temporally limiting *Ptgs2* expression and, thus, PGE2 synthesis to a minimum period may minimize inflammation-related tissue damage during the period of ovulation. Our single-cell transcriptome analysis show that at 6 h after hCG injection, *Ptger2* (a gene encoding Prostaglandin E Receptor 2) is expressed in theca cells and interstitial cells as well as immune cells. These cells also express genes for chemokines and cytokines (i.e., *Ccl2*, *Il6*, and *Il1b*) (Figure 5A). However, *Tnf* (tumor necrosis factor alpha [TNFα]-coding gene) was expressed in only immune cells. Induction of the expression of these pro-inflammatory genes in those cells in the hCG-stimulated ovary indicates that ovarian somatic cells might play a role as a mediator of ovulatory inflammation.

The regulatory role that PGR has on *Ptgs2* expression may be that PGR is induced concurrently with PTGS2 but then suppresses *Ptgs2* expression, leading to a decrease of PGE2 synthesis and, subsequently, ending the inflammation. This possibility was tested by examining whether a loss of PGR expression would elevate the degree of inflammation in the ovary. If an ovary experiences such a hyper-inflammatory condition, it might be

infiltrated with an excessive number of immune cells, such as neutrophils. To test this possibility, we examined the immune cell cluster from the single-cell RNA-seq that expressed an immune cell marker (*Ptprc*, CD45 coding gene). When the number of immune cells and expression levels of chemokines were compared, we found that the Esr2-PgrKO ovary contained twice as many immune cells as the WT (Figure 5B). Furthermore, the number of chemokine-expressing cells was increased in the mutant ovary. However, no significant difference of gene expression in immune cells was observed, primarily due to the very small number of immune cells that were used for the single-cell RNA-seq (55 cells in WT, 104 cells in Esr2-PgrKO). Therefore, we measured chemokine expression levels by RT-PCR and counted the immune cell numbers by flow cytometry by using myeloid and lymphoid lineage markers (Figure S6A). The RT-PCR results showed that *Ccl2* expression was higher in Esr2-PgrKO ovaries at hCG 6 h, but not at hCG 9 h, than in the WT ovaries (Figure 5C). Flow cytometry for immune cells showed that Esr2-PgrKO ovaries had significantly more immune cells than the WT counterparts (Figure 5D). At hCG 6 h, Esr2-PgrKO ovaries had more dendritic cells, neutrophils, monocytes and macrophages, cytotoxic T (Tc) cells, and B cells than WT ovaries. At hCG 9 h, Esr2-PgrKO ovaries contained more dendritic cells and monocytes and macrophages than WT ovaries (Figure 5D). In addition, Esr2-PgrKO showed a higher immunoreactivity to neutrophil elastase (Figure S6B), indicating a hyperinflammatory activity (Belaaouaj et al., 2000).

Loss of Pgr Expression Causes Increased Oxidative Stress and Inflammation in the Ovary

Tissues that are under an excessive inflammatory condition often undergo oxidative stress and DNA damage (Reuter et al., 2010). To determine if the loss of PGR expression induced DNA damage in granulosa cells, the degree of DNA damage was assessed using phosphorylated histone H2AX (γH2AX) as a DNA damage marker (Sharma et al., 2012). As a result, Esr2-PgrKO ovaries showed a stronger immunoreactivity to an antibody against γH2AX in the granulosa cell layer (Figure 6A). Quantitatively, the Esr2-PgrKO ovary had 2.2-fold more γH2AX-positive granulosa cells than the WT ovary at hCG 6 h (Figure 6B). To determine the cumulative ROS generation in granulosa cells, the malondialdehyde (MDA) level was assessed using an anti-MDA antibody (Ho et al., 2013). Generally, cumulus cells and mural granulosa cells were positively stained by the anti-MDA antibody. Mural granulosa cells of antral follicles of WT mice showed relatively faint immune-reactivity to MDA, whereas mural granulosa cells of the Esr2-PgrKO ovary showed relatively stronger immune-reactivity at hCG 6 and 9 h (Figure 6C). Notably, the immune-reactivity of MDA was higher at hCG 9 h than hCG 6 h, indicating that the loss of PGR expression potentially induces the excessive ROS generation and DNA damage in ovulatory mural granulosa cells. In addition, stronger immunoreactivity to the TNFα antibody was seen in the interstitium, blood vessels, and mural granulosa cell layer of the antral follicles of the Esr2-PgrKO ovary, indicating elevated inflammation when granulosa lost PGR expression (Figure 6D). In the ovary, the *Tnf* gene was exclusively expressed in immune cells (Figure 5A). Therefore, increased immune-reactivity of TNFα in the Esr2-PgrKO ovary supports the idea that the loss of PGR potentially increases immune cell recruitment and activity in the ovulatory ovary.

To date, no excessive inflammation, DNA damage, or other forms of ovarian damage have been reported in the global PgrKO mice nor have we observed such phenomena in the Esr2-PgrKO ovary. This rather contradictory phenotype may be due to the fact that the PgrKO ovary does not ovulate at all, and therefore, the ovary of either mutant mouse may not experience ovulation-induced inflammation, making either animal model inappropriate for determining the role of PGR in suppressing ovarian inflammation. As an alternative, mice with the $Pgr^{flox/wt}Esr2^{iCre/wt}$ genotype in which one *Pgr* allele was deleted in the granulosa cells was used as a model of reduced PGR expression and were named Esr2-$PgrKO^{hetero}$. They exhibit uncompromised ovulatory capacity under superovulation induction (Figure 6E). However, Esr2-$PgrKO^{hetero}$ mice showed an increased *Ptgs2* expression and decreased expression of PGR-downstream genes, such as *Adamts1*, *Fabp4*, and *Scg2*, in granulosa cells with increased neutrophil activity at hCG 6 h (Figures S7A and S7B). Furthermore, the ovaries of aged Esr2-$PgrKO^{hetero}$ mice (12 to 15 months old; n = 11 and 16 in each genotype) exhibited a higher incidence of pathologic ovarian phenotypes (Figures 6F, S7C, and S7D). In these ages, WT ovaries as well as Esr2-$PgrKO^{hetero}$ ovaries had fibrosis in the stroma and luteal interstitial cells, which is a common aging change in mice (Briley et al., 2016). Notably, hyperplasia in the ovarian surface epithelium (OSE) and adhesion of OSE cells to adjacent ovarian versa tissue were frequently and uniquely found in Esr2-$PgrKO^{hetero}$ ovaries. Oxidative stress and DNA damage associated with ovulation and inflammation have been shown contributing to neoplastic transformation of OSE cells (King and Burdette, 2011; Murdoch et al., 2001). Therefore, increased OSE hyperplasia in old Esr2-$PgrKO^{hetero}$ ovaries indicates increased cumulative tissue damage in the ovulatory process.

DISCUSSION

PGR is expressed in the entire female reproductive axis from the hypothalamus and pituitary to the ovary (Bethea and Widmann, 1998; Gal et al., 2016; Press and Greene, 1988). Blockage of the synthesis of its ligand progesterone by trilostane (Hibbert et al., 1996), inhibition of its transcriptional activity by RU486 (Loutradis et al., 1991), or the introduction of a null mutation in the *Pgr* gene (Lydon et al., 1995) result in complete ovulatory failure. These findings demonstrate a critical role that progesterone plays by PGR in regulating ovulation. The ovary has been indicated to be one of the primary sites where PGR regulates ovulation because the treatment of *Pgr*-deficient mice with an ovulatory dose of gonadotropin that should override the potential defect in the hypothalamic-pituitary axis failed to induce ovulation (Lydon et al., 1995). More direct evidence of the significant role that PGR plays in the ovulating follicle was recently provided when the ovulatory failure occurred after *Pgr* expression was silenced in the preovulatory follicle of the rhesus macaque (Bishop et al., 2016). In this study, we confirm the critical role that PGR plays in the granulosa cells by using a genetically modified animal model that is deficient of PGR expression specifically in the granulosa cells. Single-cell transcriptome analysis verified that the expression of previously reported PGR-downstream genes (Kim et al., 2009; Nallasamy et al., 2013; Robker et al., 2000) were altered in the Esr2-PgrKO ovary. Notably, unlike the absence of cyclicity in the mice that are globally deficient in PGR expression (Chappell et

al., 1997), the Esr2-PgrKO mouse cycled normally, indicating that PGR expression in the hypothalamus and pituitary is not compromised in this conditional knockout mouse.

Dysregulation of PTGS2 expression is likely associated with ovarian diseases: increased expression of PTGS2 and elevated PGE2 concentration are reported in women who experience polycystic ovarian syndrome (PCOS), ovarian hyperstimulation syndrome (OHSS), and ovarian cancer (Erkinheimo et al., 2004; Navarra et al., 1996, 2016; Schenker and Polishuk, 1976). Nonsteroidal anti-inflammatory drugs (NSAIDs) and PGE2 antagonists are known to improve OHSS symptoms (Katz et al., 1984; Várnagy et al., 2010). In human preovulatory granulosa cells, the PGR antagonists RU486 and Org-31710 increase apoptotic DNA fragmentation (Svensson et al., 2001) and overexpression of *Pgr* correlates with a favorable prognosis (Lee et al., 2005). Previous studies on the ectopic expression of PTGS2 in various ovarian diseases and disorders suggest that PTGS2 expression is needed to be adequately controlled in the ovary.

For a full transcriptional activation of the *Ptgs2* gene, two NF-κB subunits (p65 and p55) must occupy the NF-κB binding element of the *Ptgs2* promoter region. In the non-inflammatory state, NFκBIA inhibits the activity of the p65 subunit and decreases transcription of its downstream genes (Zhang et al., 2017). In the preovulatory follicles of Esr2-PgrKO mice, *Nfkbia* expression in granulosa cells was significantly lower than in the WT cells. *Nfkbia* expression was also decreased by RU486 treatment in a primary granulosa cell culture, demonstrating the requirement for PGR in *Nfkbia* expression and, therefore, its indirect regulatory role in the expression of *Ptgs2* gene. In support of this finding, gonadotropin (hCG) stimulation increased the levels of the active form of p65, acetylp65 (K310), in the granulosa cells of Esr2-PgrKO. Furthermore, our ChIP assay showed that RU486 treatment increased the binding of acetyl-p65 to the *Ptgs2* promoter in the granulosa cells, indicating that PGR decreases NF-κB binding to *Ptgs2*. NF-κB regulates the expression of a myriad of pro-inflammatory genes, including cytokines, chemokines, and adhesion molecules (Lawrence, 2009; Sun, 2017). Thus, the regulation of NF-κB activity by PGR potentially affects not only the expression of PTGS2 but also other inflammatory machinery in the ovary. Indeed, we found that the expression levels of other NF-κB-downstream genes, such as immediate early response 3 (IER3) and coagulation factor 3 (F3; also named thromboplastin) that are inflammation-response genes (Arlt and Schäfer, 2011; Mackman et al., 1991; Schmidt et al., 2014; Wu et al., 1998), were elevated in the granulosa cells of Esr2-PgrKO mice (Figures 7A and 7B). Our ChIP assay showed that the level of acetyl-p65 occupancy in the promotor regions of *Ier3* and *F3* increased upon RU486 treatment (Figures 7C and 7D).

The elevated expression of *Ptgs2* and increased PGE2 concentration caused by the loss of PGR expression in the ovaries of Esr2-PgrKO were expected to drive an excessive leukocyte inflammation in the ovary. Indeed, we saw significantly increased leukocytes, such as dendritic cells, neutrophils, monocytes and macrophages, cytotoxic T cells, and B cells, in the Esr2-PgrKO cells. An increased production of chemokine CCL2, an attractant for monocytes (Deshmane et al., 2009), neutrophils (Côté et al., 2009; Reichel et al., 2009), and macrophages (Shen et al., 2014), likely contributed to the increased leukocyte infiltration because *ccl2* expression was significantly increased in the granulosa cells of Esr2-PgrKO

compared to those of the WT. The increased neutrophil population size was reflected by stronger immunostaining by anti-neutrophil elastase, a marker of inflammatory neutrophils (Belaaouaj et al., 2000), in the Esr2-PgrKO ovaries. Together, the heightened inflammation in the Esr2-PgrKO ovary may lead to oxidative stress and DNA damage.

In aged Esr2-PgrKO^{hetero} mice, cystic follicles, neutrophil accumulation, and OSE hyperplasia were observed, indicating that impaired PGR expression during ovulation may result in cumulative damage to the ovary. In conclusion, this study shows that, in addition to its well-established role as a driver of ovulatory cascade, PGR plays another important role, namely, terminating ovulatory inflammation by silencing LH-induced *Ptgs2* expression by inducing NFκBIA expression, thereby safeguarding the ovary from repetitive ovulatory inflammations.

STAR★METHODS

KEY RESOURCES TABLE

REAGENT or RESOURCE	SOURCE	IDENTIFIER
Antibodies		
Rabbit polyclonal anti-Cyclooxygenase 2 (COX-2)	Cayman	Cat# 160106; RRID:AB_10077935
Rabbit polyclonal anti-Progesterone Receptor (PGR)	Dako	Cat# A0098; RRID:AB_2315192
Mouse monoclonal H2AX (pS139) Mouse, Alexa Fluor 647	BD Biosciences	Cat# 560447; RRID:AB_1645414
Anti-NF-κB p65 (acetyl K310) antibody - ChIP Grade	Abcam	Cat# ab19870; RRID:AB_776753
Rabbit polyclonal Anti-beta Actin	Abcam	Cat# ab8227; RRID:AB_2305186
Rabbit polyclonal anti-GAPDH	Abcam	Cat# ab9485; RRID:AB_307275
Rabbit polyclonal anti-alpha Tubulin	Abcam	Cat# ab4074; RRID:AB_2288001
Rat monoclonal anti-Neutrophil	Abcam	Cat# ab2557; RRID:AB_303154
Rabbit polyclonal anti-Neutrophil Elastase	Abcam	Cat# ab68672; RRID:AB_1658868
Goat polyclonal anti-LYVE1	R&D Systems	Cat# AF2125; RRID:AB_2297188
Rabbit polyclonal anti-Malondialdehyde (MDA)	Abcam	Cat# ab6463; RRID:AB_305484
Rat Anti-CD16 / CD32 Monoclonal (Fc Block)	BD Biosciences	Cat# 553142; RRID:AB_394657
Rat Anti-CD45 Monoclonal, PE-Cy7 Conjugated	BD Biosciences	Cat# 552848; RRID:AB_394489
Rat Anti-CD11b Monoclonal, APC-Cy7 Conjugated	BD Biosciences	Cat# 557657; RRID:AB_396772
CD11c Monoclonal (N418), PE-Cyanine5	eBioscience	Cat# 15-0114-82; RRID:AB_468717
FITC anti-mouse I-A/I-E	Biolegend	Cat# 107606; RRID:AB_313321
Rat Anti-Mouse Ly-6G Monoclonal, V450 Conjugated	BD Biosciences	Cat# 560603; RRID:AB_1727564
Brilliant Violet 421 anti-mouse Ly-6C	Biolegend	Cat# 128031; RRID:AB_2562177
PE anti-mouse/human CD45R/B220	Biolegend	Cat# 103207; RRID:AB_312992
APC Rat Anti-Mouse CD8a	BD Biosciences	Cat# 553035; RRID:AB_398527

REAGENT or RESOURCE	SOURCE	IDENTIFIER
Goat anit-rabbit, HRP-conjugated	Vector Loboratories	Cat# PK-6101; RRID:AB_2336820
Donkey anit-rat, HRP-conjugated	Jackson Immunoresearch	Cat# 712-035-150; RRID:AB_2340638
Donkey anit-rabbit, AP-conjugated	Jackson Immunoresearch	Cat# 711-055-152; RRID:AB_2340591
Chemicals, Peptides, and Recombinant Proteins		
Normal Donkey Serum	Jackson Immunoresearch	Cat# 017-000-121
Pregnant Mare Serum Gonadotropin	Sigma-Aldrich	Cat# G4877
Human chorionic gonadotropin	Sigma-Aldrich	Cat# CG10
M199 culture media	Life Technologies, Inc.	Cat# 12350–039
DMEM/F-12, HEPES	GIBCO	Cat# 11330–032
ITS Liquid Media Supplement (100 ×)	Sigma-Aldrich	Cat# I3146
Penicillin-Streptomycin (10,000 U/mL)	GIBCO	Cat# 15140–122
Sodium bicarbonate	Sigma-Aldrich	Cat# S5761
Sucrose	Sigma-Aldrich	Cat# S0389
Ethylene glycol-bis(2-aminoethylether)-N,N,N′,N′-tetraacetic acid	Sigma-Aldrich	Cat# E3889
Fetal Bovine Serum	Sigma-Aldrich	Cat# F2442
Collagenase type I	Invitrogen	Cat# 17100–017
Deoxyribonuclease I	Sigma-Aldrich	Cat# D4527
Bovine serum albumin	Sigma-Aldrich	Cat# A9418
DAB Peroxidase (HRP) Substrate Kit (with Nickel), 3,3′-diaminobenzidine	Vector Loboratories	Cat# SK-4100
Trichostatin A	Sigma-Aldrich	Cat# T8552
Nicotinamide	Sigma-Aldrich	Cat# 72340
RU486 (mifepristone)	Cayman	Cat# 10006317
Fetal Bovine Serum Stain Buffer	BD Biosciences	Cat# 554656
Benzene	Sigma-Aldrich	Cat# 270709
Ethyl acetate	Sigma-Aldrich	Cat# 270989
Methanol	Sigma-Aldrich	Cat# 34860
GelRed® Nucleic Acid Gel Stain	Biotium	Cat# 41003
Critical Commercial Assays		
Single-Cell 3′ Chromium kit V3	10X Genomics	Cat# PN-1000092
Chromatin immunoprecipitation (ChIP) assays kit	Abcam	Cat# ab500
PGE2 enzyme immunoassay (EIA) kit	Cayman	Cat# 514010
Deposited Data		
Mouse ovary single-cell RNA-seq dataset	This paper	GEO: GSE145107
Mouse granulosa cell ChIP-seq data	Dinh et al., 2019	GEO: GSE115820
Experimental Models: Organisms/Strains		
Mouse: $Pgr^{flox/flox}$, C57BL/6 background	Fernandez-Valdivia et al., 2010	N/A

REAGENT or RESOURCE	SOURCE	IDENTIFIER
Mouse: $Esr2^{iCre/iCre}$, C57BL/6 background	In house, available from Jackson laboratory	JAX stock #028717
Mouse: $Zp3^{Cre/Wt}$, C57BL/6 background	Jackson laboratory	JAX stock #003651
Oligonucleotides		
PCR primers	Table S2	N/A
Software and Algorithms		
Cell Ranger 3.0.2	10x Genomics	https://support.10xgenomics.com/single-cell-gene-expression/software/release-notes/3–0
R (v3.5)	R Core Team, 2013	https://www.r-project.org/
Seurat R package (v3.0.0)	Satija et al., 2015	https://satijalab.org/seurat/
Monocle R package (v2.10.1)	Trapnell et al., 2014	http://cole-trapnell-lab.github.io/monocle-release/
Uniform Manifold Approximation and Projection (UMAP)	McInnes et al., 2018	
Hamamatsu NDP viewer V2	Hamamatsu Photonics	https://www.hamamatsu.com/us/en/product/type/U12388-01/index.html
ImageJ	Schneider et al., 2012	https://imagej.nih.gov/ij/plugins/cell-counter.html
FCS Express 6	De Novo Software	https://denovosoftware.com/
GraphPad Prism	GraphPad Software	https://www.graphpad.com/scientific-software/prism/
SPSS version 18.0	SPSS Inc.	https://www.ibm.com/analytics/spss-statistics-software

LEAD CONTACT AND MATERIALS AVAILABILITY

Further information and requests for resources and reagents should be directed to and will be fulfilled by the Lead Contact, CheMyong J. Ko (jayko@illinois.edu). Mouse lines generated in this study have been deposited to the Jackson Laboratory [B6(Cg)-$Esr2^{t\text{-}m1.1(icre)Jako}$/J, Stock No: 028717]. This study did not generate new unique reagents.

EXPERIMENTAL MODEL AND SUBJECT DETAILS

Ethics statement—This study was carried out in accordance with the recommendations in the Guide for the Care and Use of Laboratory Animals of the National Institutes of Health. Animal protocols were approved by the University of Illinois Animal Care and Use Committee (Protocols: 11205 and 14222), and all efforts were made to minimize animal suffering. Animal models generated in this study will be made readily available to the research community.

Generation of mutant mice—All mice used were of the C57BL/6 genetic background, bred at the University of Illinois Division of Animal Resources and maintained under controlled lighting (14h light/10h dark) with continuous access to food and water. The *Pgr* gene was selectively ablated in Esr2-expressing cells by crossbreeding floxed Pgr mice ($Pgr^{flox/flox}$) (Fernandez-Valdivia et al., 2010) with transgenic mice that express Cre

recombinase under the Esr2 promoter ($Esr2^{iCre}$) (Cacioppo et al., 2016). Mice with the genotype $Pgr^{flox/flox}Esr2^{iCre}$ were generated by successive backcrossing of F1 generation mice with $Pgr^{flox/flox}$mice and are named herein as Esr2-PgrKO (*Esr2* expressing cell-specific *Pgr* knockout). Mice with the genotype $Pgr^{flox/wt}Esr2^{iCre}$ were generated by successive backcrossing of F1 generation mice with WT mice and are named herein as Esr2-$PgrKO^{hetero}$. The deletion of the *Pgr* gene in granulosa cells was confirmed by immunohistochemistry with anti-PGR antibody and RT-PCR for *Pgr* mRNA. Mice with the genotype $Pgr^{-/-}$ (global *Pgr* knockout; gPgrKO) were generated by successive backcrossing of F1 generation mice from $Pgr^{flox/flox}$ and $ZP3^{Cre}$ litters.

Genotyping—Mouse genotypes were determined by PCR. Tissue from the ear pinna was obtained by an ear punch, and DNA was extracted with an Easy DNA kit according to the manufacturer's instructions. Amplification of the floxed *Pgr* gene was performed as previously described (Gal et al., 2016). Previously described methods were used to determine hetero- or homozygous for Esr2-iCre (Cacioppo et al., 2016). PCR amplicons were run on a 2% agarose gel with GelRed® Nucleic Acid Gel Stain at 100 mV for 25 min and visualized under UV light.

Superovulation—At postnatal day (PND) 25, female mice were superovulated by intraperitoneal injection of 5 IU pregnant mare's serum gonadotropin (PMSG) and 48 h later the mice were additionally injected with 5 IU human chorionic gonadotropin (hCG).

METHOD DETAILS

Ovulatory capacity measurement and fertility assay—The mice were euthanized at 20 and 48 h after the injection of hCG for quantification of ovulated oocytes and observation for corpora lutea, respectively. Ovulated oocytes were counted from the oviduct. Fertility of 2–8-month-old wild-type (WT) and Esr2-PgrKO mice was determined by housing a proven breeder male with one Esr2-PgrKO and one WT female for 10 days. Cages were inspected daily for presence and size of a litter. The final outcome of the fertility test was determined after 30 days. Fertility percent was calculated as the number of females that gave birth divided by the total number of females in each group.

Ovarian tissue dissociation—Ovaries were collected from WT and Esr2-PgrKO mice at 6 h after hCG injection and kept in 1 mL of cold M199 suppemented with 10% FBS. After removing ovarian versa, remained tissues were dissociated into single cells by 2 mL of collagenase digestion solution containing 3.5 U of collagenase type I, 1000 U of deoxyribonuclease I, and 40 mg of BSA in M199 media at 37 °C for 30 min. Digested tissue was further dissociated with gentle pipetting using flamed glass pipet. Cellular aggregates were removed by straining cells through a 40 μm filter. Single-cells were recovered in cold M199 supplemented with 10% FBS and subjected to single-cell library construction.

Granulosa cell isolation—Granulosa cells were isolated by a follicular puncture from PMSG (10 IU, 48 h)-primed PND 27 immature mice (Orly and Sato, 1979; Park-Sarge and Mayo, 1994). Ovaries were collected in cold serum-free 4F medium containing 15 mM HEPES (pH 7.4), 50% DMEM, and 1X ITS (0.01 mg/ml recombinant human insulin, 5.5

μg/ml human transferrin, and 5 ng/ml sodium selenite), and antibiotics (50 IU/ml penicillin and 50 μg/ml streptomycin). Ovaries were incubated in 4F medium containing 0.5 M sucrose and 10 mM EGTA for 20–30 min in a 37°C incubator. After washing with a fresh 4F medium, follicles were punctured using 23-gauge needles under a dissection microscope. Cells were collected and washed with cold 4F medium, then counted using Tali Image-Based Cytometer (Invitrogen, Carlsbad, CA). Cells were plated in 4F medium supplemented with 5% fetal bovine serum (FBS) at a density of approximately 3×10^5 cells per well in 24-well culture dish and incubated in the humidified atmosphere of 5% CO_2 at 37°C. Three hours later, cells were treated with hCG alone or hCG+RU486 (mifepristone) combination in the fresh 4F medium. Cells and culture media were harvested by centrifuge (300 xg, 5 min) at the time required for each experiment and kept in −80°C until use.

Single cell library preparation—Single-cell 3′ cDNA libraries were prepared at the DNA Services laboratory of the Roy J. Carver Biotechnology Center at the University of Illinois at Urbana-Champaign. For each genotype, WT and Esr2-PgrKO, we used 8 ovaries were collected from 4-different mice in each group. From each ovary, we isolated about 500,000 cells. The single-cells from each of the ovaries were pooled to together. Single-cell suspensions with a viability of 97% (WT-hCG6h) and 88% (KO-hCG6h) by Trypan Blue staining on the TC-20 (Bio-Rad Laboratories, Inc. CA) were converted into individually barcoded cDNA libraries with the Single-Cell 3′ Chromium kit version 3 from 10X Genomics (Pleasanton, CA) following the manufacturer's protocols. Total 3,200 cells (approximately 0.6% of total cells of an ovary) were used for library construction and sequencing. The 10X Chromium instrument separates thousands of single cells into Gel Bead Emulsions (GEMs) that add a barcode to the mRNA from each individual cell. Following ds-cDNA synthesis, individually barcoded libraries compatible with the Illumina chemistry were constructed. The final libraries were quantitated on Qubit and the average size determined on the AATI Fragment Analyzer (Advanced Analytics, Ames, IA). Libraries were pooled evenly, and the final pool was diluted to 5nM concentration and further quantitated by qPCR on a Bio-Rad CFX Connect Real-Time System (Bio-Rad Laboratories, Inc. CA). The final library pool was sequenced on one lane of an Illumina NovaSeq 6000 S4 flowcell as paired-reads with 28 cycles for read 1, 8 cycles for the index read, and 150 cycles for read 2. Basecalling and demultiplexing of raw data was done with the mkfastq command of the software Cell Ranger 3.0.2 (10x Genomics).

Library preprocessing—Sequencing output was processed through the Cell Ranger 3.0.1 mkfastq and count pipelines using default parameters. Reads were quantified using the mouse GRCm38 genome assembly with Gencode annotation release M20 (without haplotypes and alternative loci). Total of 3,266 and 3,155 single cells were called by cellranger count using default settings for WT and Esr2-PgrKO samples, respectively. Mean raw reads per cell were 164,356 and 167,346 in each sample. Median genes per cell were 4,976 and 4,650 in each sample. Further analysis was performed in R (v3.5.2) using the Seurat package (v3.0.0) (Satija et al., 2015) and Monocle (v2.10.1) (Trapnell et al., 2014).

Normalization, identification of cell types and differential gene expression analysis—The analysis in this section was perform using Seurat package (Satija et al.,

2015). Feature barcode matrices from WT and Esr2-PgrKO were imported using Read10x() and CreateSeuratObject(). For each cell, a minimum expression of 500 genes was applied to filtered uninformative cells. For each gene, a minimum of 5 cells expression was applied. After log-normalization using NormalizeData(), two datasets were than integrated following FindIntegrationAnchors() and IntegrateData() procedure with the first 20 principal components for weighting. Dimensionality reduction and visualization for the 10x data was performed using Uniform Manifold Approximation and Projection (UMAP) for cells (McInnes et al., 2018). The first 20 principle components of the high-variance genes were used as input for the python implementation of the UMAP algorithm with the following default settings. Clustering on the UMAP embedding was performed using FindClusters()with 'resolution = 0.5′. Cells were grouped by WT and Esr2-PgrKO. Conserved marker genes between the groups were detected from each cluster. Ovarian cell types were determined by known cell type-specific marker genes (Figure S4). Cell type-specific differential gene expression between WT and Esr2-PgrKO was determined by Find-Markers() and visualized by Featureplot() and Vlnplot(). Differential gene expression between WT and Esr2-PgrKO was tested by default 'bimod' likelihood ratio test using FindMarkers() (cut-off, avg_logFC > 0.25, avg_logFC < −0.25, p_val_adj < 0.05) (McDavid et al., 2013; Satija et al., 2015).

Trajectory analysis—Cell trajectory by pseudotime for mural granulosa cells were performed using *Ube2c*-negative granulosa cells under Monocle2 (Trapnell et al., 2014) package. For pseudotemporal analysis, the normalized data from the indicated clusters calculated in Seurat was directly imported into Monocle2 (Trapnell et al., 2014). Mural granulosa cells were visualizedby t-SNE (num_dim = 25). Differentially expressed genes in each cluster ordered by q-value and top 1,000 genes were used for ordering cells. Dimensionality reduction was performed by reduceDimension() function with DDRTree method. Differential expression tests for each gene was performed by likelihood ratio tests and each cells were assigned to branches by branchTest(). Gene expression levels in each branch were visualized by plot_genes_branched_pseudotime().

qPCR—Ovaries were collected from the PND 27 females at 0, 3, 6, or 9 h after hCG injection and subjected to RT-PCR analysis. PCR primers used in this study are presented in Table S2. Fluorescence was measured using the ABI prism 7500 quantitative real-time thermocycler (Applied Biosystems). Results are expressed as fold differences in relative gene expression with respect to control group. Total RNA was extracted using RNAqueous®-Micro Kit (Ambion® by Life Technologies, Carlsbad, CA) according to the manufacturer's protocol. The same procedure was applied for RNA extraction from cultured cells. Concentrations of RNA were measured with a NanoDrop 1000 spectrophotometer (Thermo Scientific, Waltham, MA) and diluted to equal concentrations. RNA was reverse transcribed using a high capacity cDNA reverse transcription kit (Applied Biosynthesis, Foster City, CA). PCR reactions were performed with Power SYBR® Green PCR Master Mix (Applied Biosystems) according to the manufacturer's protocol.

Western-blot—To detect PGR protein from whole ovary tissue, ovaries were used. To detect acetyl p65 protein from cultured granulosa cell, cells were washed with cold PBS and

treated with protein extraction buffer containing 10 μM trichostatin A (TSA) and 10 mM nicotinamide (NAM). Tissues were were homogenized in RIPA buffer (89900; Thermo Scientific, Rockford, IL) containing a protease inhibitor cocktail (Roche). Then the homogenates were sonicated and centrifuged at 12,000xg for 10 min at 4°C. The supernatant was collected and protein concentration determined using a BCA Protein Assay kit (Bio-Rad). Protein samples were mixed with sample buffer containing 0.15 M dithiothreitol, boiled for 5 min, and clear supernatants were resolved on 10% SDS-PAGE gels. Following electrophoretic transfer to a PVDF membrane (Amersham Bioscience), the membrane was blocked overnight at 4°C in Tris-buffered saline with Tween-20 (TBST; 50 mM Tris-Cl [pH 7.4], 150 mM NaCl, and 0.1% Tween-20) containing 7% skim milk. After rinsing with TBST three times for 20 min each time, the membrane was incubated with the rabbit polyclonal antibody against acetyl-P65 (ab19870; 1:1000; Abcam, Cambridge, MA), PGR (A0098; 1:1000; Dako) or PTGS2 (160106, Cayman, Ann Arbor, MI) diluted in the TBST including 5% skim milk during an overnight at 4°C. As an internal control, rabbit anti-GAPDH antibody (ABS16; Millipore, Temecula, CA, 1:2000) was also used as a probe. After rinsing with TBST three times for 20 min each time, the membrane was incubated with the goat antirabbit IgG conjugated with peroxidase (111-035-144; Jackson ImmunoResearch Laboratories, West Grove, PA) diluted in 5% skim milk in TBST (1:2000) for 1h. The signals were detected using an enhanced chemiluminescence (ECL) kit (Amersham Biosciences, Piscataway, NJ).

Histology and immunohistochemistry—Mice were humanely euthanized by CO_2 asphyxiation followed by cervical dislocation. Collected tissue was immediately fixed in 4% paraformaldehyde for 24 h. Tissues were washed with ethanol, processed, and embedded in paraffin wax. Paraffin-embedded tissue blocks were sectioned 6 mm thickness. For general histological observation, slides were stained with hematoxylin and eosin (HE) staining. We performed picrosirius red (PSR) staining to detect interstitial collagen. Briefly, deparaffinized sections were hydrated and stained with 0.1% PSR for 90 min. HE and PSR-stained slides were then dehydrated and mounted. Immunolabeling of each antibody was done in the following manner: deparaffinization was followed by heat-induced antigen retrieval in 10 mM sodium citrate buffer (pH 6.0), endogenous peroxide quenching in 3% H_2O_2, and antibody and endogenous biotin blockage by 5% goat serum with avidin (200 μl/ml; SP-2001, Vector Labs, Burlingame, CA). Incubation of the primary rabbit anti-mouse PGR antibody (A0098, Dako, Carpinteria, CA), primary rabbit anti-mouse PTGS2 antibody (Cayman), primary rat anti-neutrophil antibody (ab2557, Abcam), primary rabbit anti-neutrophil elastase antibody (ab68672, Abcam), or primary rabbit anti-MDA antibody (ab6463, Abcam) and biotin (200 μl/ml; SP-2001, Vector labs) was followed by incubation with a secondary biotinylated goat anti-rabbit antibody (Vectastain ABC kit, Vector labs) and avidin-biotin complex solution (Vectastain Elite ABC kit, Vector labs) at room temperature. 3,3′-diaminobenzidine (DAB; SK-4100, Vector Labs) or alkaline phosphatase substrate kit (SK-5100; Vector labs) was applied until it developed optimal color. Slides were then counter-stained with hematoxylin, mounted, and imaged with an Olympus BX51 microscope. For immunofluorescence labeling of phosphorylated histone H2AX (γH2AX) and tumor necrosis factor alpha (TNFα) expression in the preovulatory ovary, paraffin-embedded tissue blocks were sectioned to 6 mm thickness. After hydration, immunolabeling

of each antibody was done by heat-induced antigen retrieval in 10 mM Tris-EDTA buffer (pH 9.0), endogenous peroxide quenching in 3% H_2O_2, and blockage by 5% donkey serum. Slides were incubated with the Alexa Fluor 647-conjugated anti-H2AX (pS139) antibody (554418, BD Biosciences) or FITC-conjugated anti-TNFα antibody (560447, BD Biosciences) diluted 1:100 in 2.5% normal donkey serum in a humidified chamber overnight at 4°C. After washing three times, nuclear staining and mounting were conducted with ProLong Gold (Invitrogen, Eugene, OR) containing DAPI. Slides were observed under a confocal microscope- equipped (A1, Nikon, Japan) imaging system.

Chromatin immunoprecipitation—The chromatin immunoprecipitation (ChIP) assays were performed using a ChIP kit (ab500, Abcam) according to the manufacturer's instructions. The targeting region of proximal ChIP primers was spanned the NF-κB binding site (—401/−393 and —93/−88) in the promoter of mouse *Ptgs2* gene (Klein et al., 2007). NF-κB binding site on *Ier3* and *F3* genes were predicted by MotifMap system (http://motifmap.ics.uci.edu/) and reference mouse genome sequence (mm9). For prediction of NF-κB binding site, we used ± 5000 bp from transcription start site (TSS) of each gene. The targeting region of proximal ChIP primers was spanned the NF-κB binding sites were —112/−101 bp from *Ier3* TSS and —113/−103 bp from *F3* TSS, respectively. Fluorescence of amplicons was measured using the ABI prism 7500 quantitative real-time thermocycler (Applied Biosystems). Results are expressed as fold differences in relative amplification with respect to the input control. The chromatin was cross-linked by treating the cells with 1% formaldehyde for 10 min at RT. After quenching the formaldehyde using glycine, cells were lysed under 4°C. The cross-linked chromatin was fragmented (200–1000 bp) by sonication. The rabbit polyclonal anti-acetyl-P65 antibody (ab19870; Abcam), negative control rabbit immunoglobulin fraction (negative control; X0936, Dako) and rabbit polyclonal anti-histone H3 antibody (positive control; ab1791, Abcam) at a 10 μg/ml concentration were used for immunoprecipitation, respectively. The DNA was then purified and kept in —80°C until use. PCR with the ChIP primers (Table S1) was performed as follows: 34 cycles of denaturation for 30 s at 95°C, annealing for 30 s at 60°C, and extension for 50 s at 72°C.

Flow cytometry—Single cell suspensions of ovary cells were prepared by modifying a method previously described (Oakley et al., 2010). Ovaries were collected from WT and Esr2-PgrKO mice at 6 and 9 h after hCG injection and dissociated by 2 mL of collagenase digestion solution containing 3.5 U of collagenase type I (17100–017; Invitrogen), 1000 U of deoxyribonuclease I (D4527; Sigma), and 40 mg of BSA (017K0723; Sigma) in H-199 media (12350–039; Life Technologies, Inc.) at 37°C for 30 min. Dissociated cells (1×10^6 cells) were washed and stained according to the manufacturer's protocol with the following antibodies alone or in varying combinations: CD16/CD32 (Mouse BD Fc Block; 553142, BD Biosciences, San Jose, CA) CD45-PE/Cy7 (552848, BD Biosciences), CD11b-APC/Cy7 (557657, BD Biosciences), CD11c-PE/Cy5 (15-0114-82, eBioscience, San Diego, CA), I-A/I-E (MHCII)-FITC (562009, BD Biosciences), Ly6G-Horizon V450 (560603, BD Biosciences), Ly6C-Brilliant Violet 450 (128033, Biolegend, San Diego, CA), CD45R/B220-PE (553089, BD Biosciences), and CD8a-APC (553035, BD Biosciences). For surface marker staining, DPBS (pH 7.4) containing heat-inactivated FBS and < 0.09% sodium azide

(554656, BD Biosciences) was used as staining buffer. Stained samples were analyzed by flow cytometry (BD LSR II; BD Biosciences). Data analysis was performed using FCS Express 6 (*De Novo* Software, Los Angeles, CA).

PGE2 measurement—The concentration of PGE2 in the whole ovary was determined using an enzyme immunoassay (EIA) kit (Cayman). Frozen tissues were homogenized and subjected to PGE2 purification using a silica-based column. PGE2 was eluted from the column using benzene:ethyl acetate:methanol (60:40:2) solution, then dried under the nitrogen steam. Eluted contents were dissolved in ELISA buffer which was provided from EIA kit (Cayman). The PGE2 concentration was determined according to the instructions provided with the kit. PGE2 concentration in each ovary tissue was presented as pg/mg ovary.

QUANTIFICATION AND STATISTICAL ANALYSIS

Image analysis/Immunostaining quantification—γH2AX were detected by immunofluorescence labeling in ovary sections. Total and γH2AX-positive cell number was counted by ImageJ software. Data were presented by γH2AX-positive/total cell ratio. For quantitative analysis for occurrence frequency of γH2AX-positive granulosa cells, five different antral follicles in five different WT and Esr2-PgrKO were used, respectively. MDA were detected by immunohistochemistry labeling in ovary sections. The intensity of staining in mural granulosa cell layer was quantified by ImageJ software. Data were presented by log(max/mean intensity). Three to five different antral follicles in three to four different WT and Esr2-PgrKO were used for quantification of MDA intensity.

Statistical analysis—All sample sizes can be found in figure legends. Data analyses were performed using GraphPad Prism and SPSS version 18.0. Continuous data were tested for normal distribution by a Shapiro-Wilk test. All normally distributed continuous data were analyzed with parametric tests (Student’s t test or one-way ANOVA with Tukey post hoc test). Data are graphically presented as the mean and standard deviation. Statistical significance was accepted when P values were lower than 0.05.

DATA AND CODE AVAILABILITY

The accession number for the FastQ files of the single-cell RNA-seq libraries reported in this paper is GEO: GSE145107. The source code of the analysis is publicly available on GitHub at https://github.com/cjpark85/Mouse-Ovary-PGR.

Supplementary Material

Refer to Web version on PubMed Central for supplementary material.

ACKNOWLEDGMENTS

We thank Dr. C.L. Wright (Roy J. Carver Biotechnology Center, University of Illinois at Urbana-Champaign), Dr. C.J. Fields (HPCBio, University of Illinois at Urbana-Champaign), Dr. J. Drnevich (HPCBio), and Dr. M. Tseng (HPCBio) for their assistance in performing single-cell RNA sequencing and analyzing data. This work was supported by grants from the National Institutes of Health (NIH) (HD071875 and HD094296 to C.J.K.; HD042311 to J.P.L.).

REFERENCES

Akison LK, and Robker RL (2012). The critical roles of progesterone receptor (PGR) in ovulation, oocyte developmental competence and oviductal transport in mammalian reproduction. Reprod. Domest. Anim 47, 288–296.

Arlt A, and Schäfer H (2011). Role of the immediate early response 3 (IER3) gene in cellular stress response, inflammation and tumorigenesis. Eur. J. Cell Biol 90, 545–552. [PubMed: 21112119]

Belaaouaj A, Kim KS, and Shapiro SD (2000). Degradation of outer membrane protein A in Escherichia coli killing by neutrophil elastase. Science 289, 1185–1188. [PubMed: 10947984]

Bethea CL, and Widmann AA (1998). Differential expression of progestin receptor isoforms in the hypothalamus, pituitary, and endometrium of rhesus macaques. Endocrinology 139, 677–687. [PubMed: 9449641]

Bishop CV, Hennebold JD, Kahl CA, and Stouffer RL (2016). Knockdown of Progesterone Receptor (PGR) in Macaque Granulosa Cells Disrupts Ovulation and Progesterone Production. Biol. Reprod 94, 109. [PubMed: 26985003]

Boots CE, and Jungheim ES (2015). Inflammation and Human Ovarian Follicular Dynamics. Semin. Reprod. Med 33, 270–275. [PubMed: 26132931]

Briley SM, Jasti S, McCracken JM, Hornick JE, Fegley B, Pritchard MT, and Duncan FE (2016). Reproductive age-associated fibrosis in the stroma of the mammalian ovary. Reproduction 152, 245–260. [PubMed: 27491879]

Cacioppo JA, Koo Y, Lin PC, Osmulski SA, Ko CD, and Ko C (2016). Generation of an estrogen receptor beta-iCre knock-in mouse. Genesis 54, 38–52. [PubMed: 26663382]

Chappell PE, Lydon JP, Conneely OM, O'Malley BW, and Levine JE (1997). Endocrine defects in mice carrying a null mutation for the progesterone receptor gene. Endocrinology 138, 4147–4152. [PubMed: 9322923]

Chappell PE, Schneider JS, Kim P, Xu M, Lydon JP, O'Malley BW, and Levine JE (1999). Absence of gonadotropin surges and gonadotropinreleasing hormone self-priming in ovariectomized (OVX), estrogen (E2)-treated, progesterone receptor knockout (PRKO) mice. Endocrinology 140, 3653–3658. [PubMed: 10433223]

Choi Y, Park JY, Wilson K, Rosewell KL, Brännström M, Akin JW, Curry TE Jr., and Jo M (2017). The expression of CXCR4 is induced by the luteinizing hormone surge and mediated by progesterone receptors in human preovulatory granulosa cells. Biol. Reprod 96, 1256–1266. [PubMed: 28595291]

Côté SC, Pasvanis S, Bounou S, and Dumais N (2009). CCR7-specific migration to CCL19 and CCL21 is induced by PGE(2) stimulation in human monocytes: Involvement of EP(2)/EP(4) receptors activation. Mol. Immunol 46, 2682–2693. [PubMed: 19545899]

Davis BJ, Lennard DE, Lee CA, Tiano HF, Morham SG, Wetsel WC, and Langenbach R (1999). Anovulation in cyclooxygenase-2-deficient mice is restored by prostaglandin E2 and interleukin-1beta. Endocrinology 140, 2685–2695. [PubMed: 10342859]

Deshmane SL, Kremlev S, Amini S, and Sawaya BE (2009). Monocyte chemoattractant protein-1 (MCP-1): an overview. J. Interferon Cytokine Res 29, 313–326. [PubMed: 19441883]

DeWitt DL (1991). Prostaglandin endoperoxide synthase: regulation of enzyme expression. Biochim. Biophys. Acta 1083, 121–134. [PubMed: 1903657]

Dinh DT, Breen J, Akison LK, DeMayo FJ, Brown HM, Robker RL, and Russell DL (2019). Tissue-specific progesterone receptor-chromatin binding and the regulation of progesterone-dependent gene expression. Sci. Rep 9, 11966. [PubMed: 31427604]

Duffy DM, Ko C, Jo M, Brannstrom M, and Curry TE (2019). Ovulation: Parallels With Inflammatory Processes. Endocr. Rev 40, 369–416. [PubMed: 30496379]

Erkinheimo TL, Lassus H, Finne P, van Rees BP, Leminen A, Ylikorkala O, Haglund C, Butzow R, and Ristimaki A (2004). Elevated cyclooxygenase-2 expression is associated with altered expression of p53 and SMAD4, amplification of HER-2/neu, and poor outcome in serous ovarian carcinoma. Clin. Cancer Res 10, 538–545. [PubMed: 14760075]

Espey LL (1980). Ovulation as an inflammatory reaction—a hypothesis. Biol. Reprod 22, 73–106. [PubMed: 6991013]

Espey LL (1994). Current status of the hypothesis that mammalian ovulation is comparable to an inflammatory reaction. Biol. Reprod 50, 233–238. [PubMed: 8142541]

Fernandez-Valdivia R, Jeong J, Mukherjee A, Soyal SM, Li J, Ying Y, Demayo FJ, and Lydon JP (2010). A mouse model to dissect progesterone signaling in the female reproductive tract and mammary gland. Genesis 48, 106–113. [PubMed: 20029965]

Gal A, Lin PC, Cacioppo JA, Hannon PR, Mahoney MM, Wolfe A, Fernandez-Valdivia R, Lydon JP, Elias CF, and Ko C (2016). Loss of Fertility in the Absence of Progesterone Receptor Expression in Kisspeptin Neurons of Female Mice. PLoS One 11, e0159534. [PubMed: 27441639]

Hardy DB, Janowski BA, Corey DR, and Mendelson CR (2006). Progesterone receptor plays a major antiinflammatory role in human myometrial cells by antagonism of nuclear factor-kappaB activation of cyclooxygenase 2 expression. Mol. Endocrinol 20, 2724–2733. [PubMed: 16772530]

Hibbert ML, Stouffer RL, Wolf DP, and Zelinski-Wooten MB (1996). Midcycle administration of a progesterone synthesis inhibitor prevents ovulation in primates. Proc. Natl. Acad. Sci. USA 93, 1897–1901. [PubMed: 8700855]

Ho E, Karimi Galougahi K, Liu CC, Bhindi R, and Figtree GA (2013). Biological markers of oxidative stress: Applications to cardiovascular research and practice. Redox Biol 1, 483–491. [PubMed: 24251116]

Iversen L, Fielding S, Lidegaard Ø, Mørch LS, Skovlund CW, and Hannaford PC (2018). Association between contemporary hormonal contraception and ovarian cancer in women of reproductive age in Denmark: prospective, nationwide cohort study. BMJ 362, k3609. [PubMed: 30257920]

Jabbour HN, Sales KJ, Catalano RD, and Norman JE (2009). Inflammatory pathways in female reproductive health and disease. Reproduction 138, 903–919. [PubMed: 19793840]

Jablonka-Shariff A, and Olson LM (1998). The role of nitric oxide in oocyte meiotic maturation and ovulation: meiotic abnormalities of endothelial nitric oxide synthase knock-out mouse oocytes. Endocrinology 139, 2944–2954. [PubMed: 9607805]

Jia D, Nagaoka Y, Katsumata M, and Orsulic S (2018). Inflammation is a key contributor to ovarian cancer cell seeding. Sci. Rep 8, 12394. [PubMed: 30120290]

Johnson LA, Prevo R, Clasper S, and Jackson DG (2007). Inflammationinduced uptake and degradation of the lymphatic endothelial hyaluronan receptor LYVE-1. J. Biol. Chem 282, 33671–33680. [PubMed: 17884820]

Katz Z, Lancet M, Borenstein R, and Chemke J (1984). Absence of teratogenicity of indomethacin in ovarian hyperstimulation syndrome. Int. J. Fertil 29, 186–188. [PubMed: 6152259]

Kidane D, Chae WJ, Czochor J, Eckert KA, Glazer PM, Bothwell AL, and Sweasy JB (2014). Interplay between DNA repair and inflammation, and the link to cancer. Crit. Rev. Biochem. Mol. Biol 49, 116–139. [PubMed: 24410153]

Kim J, Bagchi IC, and Bagchi MK (2009). Control of ovulation in mice by progesterone receptor-regulated gene networks. Mol. Hum. Reprod 15, 821–828. [PubMed: 19815644]

King SM, and Burdette JE (2011). Evaluating the progenitor cells of ovarian cancer: analysis of current animal models. BMB Rep 44, 435–445. [PubMed: 21777513]

Klein T, Shephard P, Kleinert H, and Kömhoff M (2007). Regulation of cyclooxygenase-2 expression by cyclic AMP. Biochim. Biophys. Acta 1773, 1605–1618. [PubMed: 17945363]

Kodaman PH, and Behrman HR (2001). Endocrine-regulated and protein kinase C-dependent generation of superoxide by rat preovulatory follicles. Endocrinology 142, 687–693. [PubMed: 11159840]

Kubota K, Cui W, Dhakal P, Wolfe MW, Rumi MA, Vivian JL, Roby KF, and Soares MJ (2016). Rethinking progesterone regulation of female reproductive cyclicity. Proc. Natl. Acad. Sci. USA 113, 4212–4217. [PubMed: 27035990]

Lawrence T (2009). The nuclear factor NF-kappaB pathway in inflammation. Cold Spring Harb. Perspect. Biol 1, a001651. [PubMed: 20457564]

Lee P, Rosen DG, Zhu C, Silva EG, and Liu J (2005). Expression of progesterone receptor is a favorable prognostic marker in ovarian cancer. Gynecol. Oncol 96, 671–677. [PubMed: 15721410]

Loutradis D, Bletsa R, Aravantinos L, Kallianidis K, Michalas S, and Psychoyos A (1991). Preovulatory effects of the progesterone antagonist mifepristone (RU486) in mice. Hum. Reprod 6, 1238–1240. [PubMed: 1752924]

Lydon JP, DeMayo FJ, Funk CR, Mani SK, Hughes AR, Montgomery CA Jr., Shyamala G, Conneely OM, and O'Malley BW (1995). Mice lacking progesterone receptor exhibit pleiotropic reproductive abnormalities. Genes Dev 9, 2266–2278. [PubMed: 7557380]

Mackman N, Brand K, and Edgington TS (1991). Lipopolysaccharide-mediated transcriptional activation of the human tissue factor gene in THP-1 monocytic cells requires both activator protein 1 and nuclear factor kappa B binding sites. J. Exp. Med 174, 1517–1526. [PubMed: 1744583]

McDavid A, Finak G, Chattopadyay PK, Dominguez M, Lamoreaux L, Ma SS, Roederer M, and Gottardo R (2013). Data exploration, quality control and testing in single-cell qPCR-based gene expression experiments. Bioinformatics 29, 461–467. [PubMed: 23267174]

McInnes L, Healy J, and Melville J (2018). Umap: Uniform manifold approximation and projection for dimension reduction. arXiv, arXiv:180203426. https://arxiv.org/abs/1802.03426.

Mendelson CR (2009). Minireview: fetal-maternal hormonal signaling in pregnancy and labor. Mol. Endocrinol 23, 947–954. [PubMed: 19282364]

Morris JK, and Richards JS (1995). Luteinizing hormone induces prostaglandin endoperoxide synthase-2 and luteinization in vitro by A-kinase and C-kinase pathways. Endocrinology 136, 1549–1558. [PubMed: 7895665]

Murdoch WJ, Townsend RS, and McDonnel AC (2001). Ovulationinduced DNA damage in ovarian surface epithelial cells of ewes: prospective regulatory mechanisms of repair/survival and apoptosis. Biol. Reprod 65, 1417–1424. [PubMed: 11673258]

Nagaraja AS, Dorniak PL, Sadaoui NC, Kang Y, Lin T, Armaiz-Pena G, Wu SY, Rupaimoole R, Allen JK, Gharpure KM, et al. (2016). Sustained adrenergic signaling leads to increased metastasis in ovarian cancer via increased PGE2 synthesis. Oncogene 35, 2390–2397. [PubMed: 26257064]

Nallasamy S, Kim J, Sitruk-Ware R, Bagchi M, and Bagchi I (2013). Ulipristal blocks ovulation by inhibiting progesterone receptor-dependent pathways intrinsic to the ovary. Reprod. Sci 20, 371–381. [PubMed: 23012316]

Natraj U, and Richards JS (1993). Hormonal regulation, localization, and functional activity of the progesterone receptor in granulosa cells of rat preovulatory follicles. Endocrinology 133, 761–769. [PubMed: 8344215]

Navarra P, Andreani CL, Lazzarin N, Pierro E, Mirtella A, Lanzone A, and Mancuso S (1996). Increased production and release of prostaglandin-E2 by human granulosa cells from polycystic ovaries. Prostaglandins 52, 187–197. [PubMed: 8908619]

Needleman P, Turk J, Jakschik BA, Morrison AR, and Lefkowith JB (1986). Arachidonic acid metabolism. Annu. Rev. Biochem 55, 69–102. [PubMed: 3017195]

Ness RB, and Cottreau C (1999). Possible role of ovarian epithelial inflammation in ovarian cancer. J. Natl. Cancer Inst 91, 1459–1467. [PubMed: 10469746]

Oakley OR, Kim H, El-Amouri I, Lin PC, Cho J, Bani-Ahmad M, and Ko C (2010). Periovulatory leukocyte infiltration in the rat ovary. Endocrinology 151, 4551–4559. [PubMed: 20591976]

Oakley OR, Frazer ML, and Ko C (2011). Pituitary-ovary-spleen axis in ovulation. Trends Endocrinol. Metab 22, 345–352. [PubMed: 21600783]

Orly J, and Sato G (1979). Fibronectin mediates cytokinesis and growth of rat follicular cells in serum-free medium. Cell 17, 295–305. [PubMed: 455465]

Park OK, and Mayo KE (1991). Transient expression of progesterone receptor messenger RNA in ovarian granulosa cells after the preovulatory luteinizing hormone surge. Mol. Endocrinol 5, 967–978. [PubMed: 1840636]

Park-Sarge OK, and Mayo KE (1994). Regulation of the progesterone receptor gene by gonadotropins and cyclic adenosine 3′,5′-monophosphate in rat granulosa cells. Endocrinology 134, 709–718. [PubMed: 8299566]

Peng XR, Hsueh AJ, LaPolt PS, Bjersing L, and Ny T (1991). Localization of luteinizing hormone receptor messenger ribonucleic acid expression in ovarian cell types during follicle development and ovulation. Endocrinology 129, 3200–3207. [PubMed: 1954899]

Press MF, and Greene GL (1988). Localization of progesterone receptor with monoclonal antibodies to the human progestin receptor. Endocrinology 122, 1165–1175. [PubMed: 3342750]

Prevo R, Banerji S, Ferguson DJ, Clasper S, and Jackson DG (2001). Mouse LYVE-1 is an endocytic receptor for hyaluronan in lymphatic endothelium. J. Biol. Chem 276, 19420–19430. [PubMed: 11278811]

Reichel CA, Rehberg M, Lerchenberger M, Berberich N, Bihari P, Khandoga AG, Zahler S, and Krombach F (2009). Ccl2 and Ccl3 mediate neutrophil recruitment via induction of protein synthesis and generation of lipid mediators. Arterioscler. Thromb. Vasc. Biol 29, 1787–1793. [PubMed: 19608967]

Renthal NE, Williams KC, and Mendelson CR (2013). MicroRNAs—mediators of myometrial contractility during pregnancy and labour. Nat. Rev. Endocrinol 9, 391–401. [PubMed: 23669656]

Reuter S, Gupta SC, Chaturvedi MM, and Aggarwal BB (2010). Oxidative stress, inflammation, and cancer: how are they linked? Free Radic. Biol. Med 49, 1603–1616. [PubMed: 20840865]

Ricciotti E, and FitzGerald GA (2011). Prostaglandins and inflammation. Arterioscler. Thromb. Vasc. Biol 31, 986–1000. [PubMed: 21508345]

Richards JS (2018). From Follicular Development and Ovulation to Ovarian Cancers: An Unexpected Journey. Vitam. Horm 107, 453–472. [PubMed: 29544640]

Richards JS, and Ascoli M (2018). Endocrine, Paracrine, and Autocrine Signaling Pathways That Regulate Ovulation. Trends Endocrinol. Metab 29, 313–325. [PubMed: 29602523]

Richards JS, Russell DL, Robker RL, Dajee M, and Alliston TN (1998). Molecular mechanisms of ovulation and luteinization. Mol. Cell. Endocrinol 145, 47–54. [PubMed: 9922098]

Richards JS, Russell DL, Ochsner S, and Espey LL (2002). Ovulation: new dimensions and new regulators of the inflammatory-like response. Annu. Rev. Physiol 64, 69–92. [PubMed: 11826264]

Robker RL, and Richards JS (1998). Hormone-induced proliferation and differentiation of granulosa cells: a coordinated balance of the cell cycle regulators cyclin D2 and p27Kip1. Mol. Endocrinol 12, 924–940. [PubMed: 9658398]

Robker RL, Russell DL, Espey LL, Lydon JP, O'Malley BW, and Richards JS (2000). Progesterone-regulated genes in the ovulation process: ADAMTS-1 and cathepsin L proteases. Proc. Natl. Acad. Sci. USA 97, 4689–4694. [PubMed: 10781075]

Satija R, Farrell JA, Gennert D, Schier AF, and Regev A (2015). Spatial reconstruction of single-cell gene expression data. Nat. Biotechnol 33, 495–502. [PubMed: 25867923]

Savant SS, Sriramkumar S, and O'Hagan HM (2018). The Role of Inflammation and Inflammatory Mediators in the Development, Progression, Metastasis, and Chemoresistance of Epithelial Ovarian Cancer. Cancers (Basel) 10, E251. [PubMed: 30061485]

Schenker JG, and Polishuk WZ (1976). The role of prostaglandins in ovarian hyperstimulation syndrome. Eur. J. Obstet. Gynecol. Reprod. Biol 6, 47–52. [PubMed: 985762]

Schmidt J, Weijdegå rd B, Mikkelsen AL, Lindenberg S, Nilsson L, and Brä nnströ m M (2014). Differential expression of inflammation-related genes in the ovarian stroma and granulosa cells of PCOS women. Mol. Hum. Reprod 20, 49–58. [PubMed: 23900753]

Schneider CA, Rasband WS, and Eliceiri KW (2012). NIH Image to ImageJ: 25 years of image analysis. Nat. Methods 9, 671–675. [PubMed: 22930834]

Sharma A, Singh K, and Almasan A (2012). Histone H2AX phosphorylation: a marker for DNA damage. Methods Mol. Biol 920, 613–626. [PubMed: 22941631]

Shen JZ, Morgan J, Tesch GH, Fuller PJ, and Young MJ (2014). CCL2-dependent macrophage recruitment is critical for mineralocorticoid receptor-mediated cardiac fibrosis, inflammation, and blood pressure responses in male mice. Endocrinology 155, 1057–1066. [PubMed: 24428529]

Shimada M, Yanai Y, Okazaki T, Yamashita Y, Sriraman V, Wilson MC, and Richards JS (2007). Synaptosomal-associated protein 25 gene expression is hormonally regulated during ovulation and is involved in cytokine/chemokine exocytosis from granulosa cells. Mol. Endocrinol 21, 2487–2502. [PubMed: 17595323]

Shukovski L, and Tsafriri A (1994). The involvement of nitric oxide in the ovulatory process in the rat. Endocrinology 135, 2287–2290. [PubMed: 7525265]

Sirois J, Simmons DL, and Richards JS (1992). Hormonal regulation of messenger ribonucleic acid encoding a novel isoform of prostaglandin endoperoxide H synthase in rat preovulatory follicles. Induction in vivo and in vitro. J. Biol. Chem 267, 11586–11592. [PubMed: 1597485]

Sirois J, Levy LO, Simmons DL, and Richards JS (1993). Characterization and hormonal regulation of the promoter of the rat prostaglandin endoperoxide synthase 2 gene in granulosa cells. Identification of functional and protein-binding regions. J. Biol. Chem 268, 12199–12206. [PubMed: 8505340]

Sirois J, Sayasith K, Brown KA, Stock AE, Bouchard N, and Doré M (2004). Cyclooxygenase-2 and its role in ovulation: a 2004 account. Hum. Reprod. Update 10, 373–385. [PubMed: 15205395]

Spanel-Borowski K (2011). Ovulation as danger signaling event of innate immunity. Mol. Cell. Endocrinol 333, 1–7. [PubMed: 21163330]

Sriraman V, Sinha M, and Richards JS (2010). Progesterone receptorinduced gene expression in primary mouse granulosa cell cultures. Biol. Reprod 82, 402–412. [PubMed: 19726735]

Sun SC (2017). The non-canonical NF-κB pathway in immunity and inflammation. Nat. Rev. Immunol 17, 545–558. [PubMed: 28580957]

Svensson EC, Markström E, Shao R, Andersson M, and Billig H (2001). Progesterone receptor antagonists Org 31710 and RU 486 increase apoptosis in human periovulatory granulosa cells. Fertil. Steril 76, 1225–1231. [PubMed: 11730755]

Trapnell C, Cacchiarelli D, Grimsby J, Pokharel P, Li S, Morse M, Lennon NJ, Livak KJ, Mikkelsen TS, and Rinn JL (2014). The dynamics and regulators of cell fate decisions are revealed by pseudotemporal ordering of single cells. Nat. Biotechnol 32, 381–386. [PubMed: 24658644]

Várnagy A, Bódis J, Mánfai Z, Wilhelm F, Busznyák C, and Koppán M (2010). Low-dose aspirin therapy to prevent ovarian hyperstimulation syndrome. Fertil. Steril 93, 2281–2284. [PubMed: 19261278]

Wei J, and Xiao GM (2013). The neuroprotective effects of progesterone on traumatic brain injury: current status and future prospects. Acta Pharmacol. Sin 34, 1485–1490. [PubMed: 24241345]

White MM, Sheffer I, Teeter J, and Apostolakis EM (2007). Hypothalamic progesterone receptor-A mediates gonadotropin surges, self priming and receptivity in estrogen-primed female mice. J. Mol. Endocrinol 38, 35–50. [PubMed: 17242168]

Wu MX, Ao Z, Prasad KV, Wu R, and Schlossman SF (1998). IEX-1L, an apoptosis inhibitor involved in NF-kappaB-mediated cell survival. Science 281, 998–1001. [PubMed: 9703517]

Yamauchi J, Miyazaki T, Iwasaki S, Kishi I, Kuroshima M, Tei C, and Yoshimura Y (1997). Effects of nitric oxide on ovulation and ovarian steroidogenesis and prostaglandin production in the rabbit. Endocrinology 138, 3630–3637. [PubMed: 9275046]

Yang F, and Bleich D (2004). Transcriptional regulation of cyclooxygenase-2 gene in pancreatic beta-cells. J. Biol. Chem 279, 35403–35411. [PubMed: 15213229]

Yang-Hartwich Y, Gurrea-Soteras M, Sumi N, Joo WD, Holmberg JC, Craveiro V, Alvero AB, and Mor G (2014). Ovulation and extra-ovarian origin of ovarian cancer. Sci. Rep 4, 6116. [PubMed: 25135607]

Zhang Q, Lenardo MJ, and Baltimore D (2017). 30 Years of NF-κB: A Blossoming of Relevance to Human Pathobiology. Cell 168, 37–57. [PubMed: 28086098]

Highlights

- Successful ovulation requires timely expression of PGR in the ovarian granulosa cells
- PGR terminates LH-surge-driven PGE2 synthesis by decreasing PTGS2 (COX-2) expression
- Impaired PGR expression leads to hyperinflammation and tissue damage in the ovary

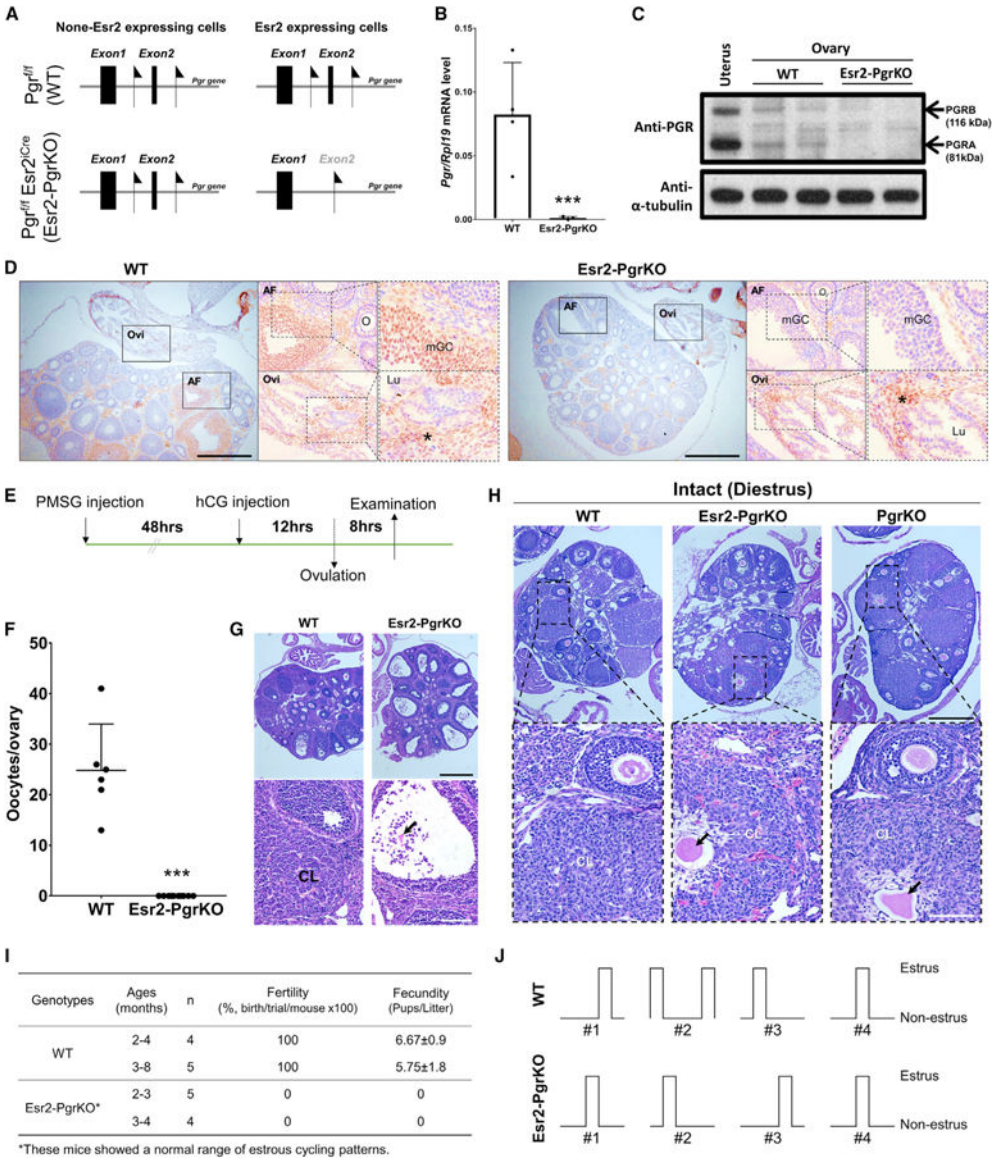

Figure 1. *Pgr* Expression Is Selectively Lost in the Granulosa Cells of the Esr2-PgrKO Ovary

(A) Location of Loxp sequence in exon 2 in the *Pgr* gene of $Pgr^{f/f}$ and double transgenic $Pgr^{f/f}Esr2^{iCre}$ mice.

(B) Ovarian *Pgr* mRNA expression in WT and Esr2-PgrKO at 3 h after hCG injection. Real-time PCR was performed using *Pgr*-specific primers. *Rpl19* was also amplified as an internal control. Error bar, SD (n = 4); ***p < 0.001 (Student's t test).

(C) PGR protein expression in WT and Esr2-PgrKO ovaries at hCG 6 h. The uterus was included as a positive control for PGR expression.

(D) Immunohistochemistry for PGR in WT and Esr2-PgrKO ovaries at hCG 6 h. Brown color represents the sites of the PGR localization. AF, antral follicles; Lu, lumen; mGC, mural granulosa cells; O, oocytes; Ovi, oviduct. Asterisks indicate the PGR-expressing interstitial cells in ovaries (scale bars, 0.5 mm).

(E) Timeline of PMSG and hCG injection for ovulation induction in 24-day-old mice.

(F) Number of ovulated oocytes was counted at 20 h after hCG injection from the oviduct. Error bar, SEM (n = 6, WT; n = 10, Esr2-PgrKO); ***p < 0.001 (Student's t test).
(G) Histology of ovaries by H&E staining at hCG 20 h. CL, corpus luteum; arrow indicates the entrapped oocyte in CL (top scale bar, 0.5 mm; bottom scale bar, 100 mm).
(H) Entrapped oocytes in corpora lutea in Esr2-PgrKO and global PgrKO ovaries. Ovaries and reproductive tract tissues were collected from 45- to 52-day-old WT, Esr2-PgrKO, and global PgrKO mice during diestrus and were subjected to H&E histology. Arrows indicate entrapped oocytes in a CL. Note the presence of the lighter staining, larger lutein cells around the oocytes compared to the granulosa cells around adjacent oocytes in developing follicles (top scale bar, 0.5 mm; bottom scale bar, 100 mm).
(I) Fertility and fecundity tested in different age groups of mice. Data presented with mean ± SEM.
(J) Representative estrous cyclicity determined by vaginal cytology for 10 days (n = 4).

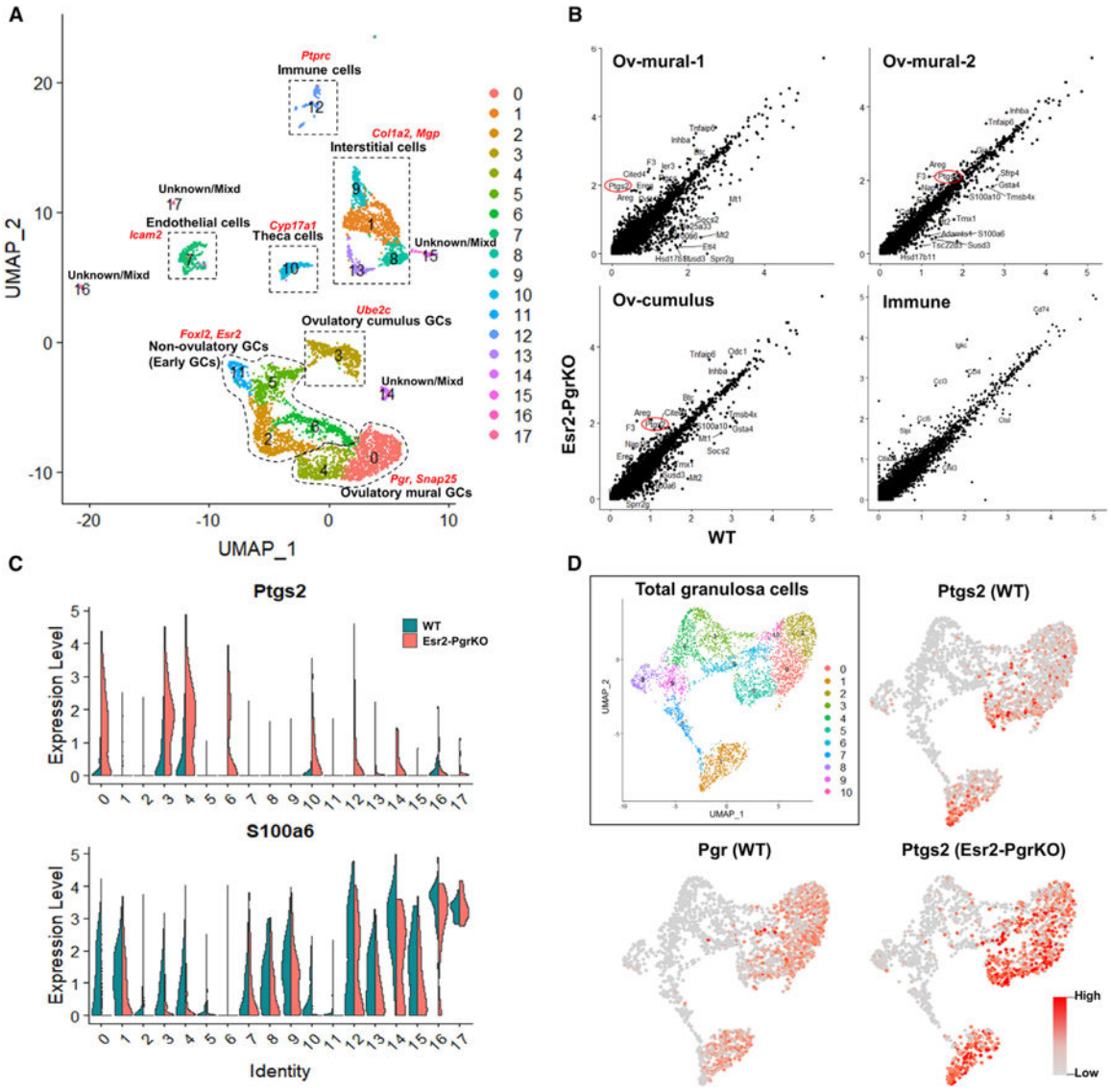

Figure 2. Upregulation of *Ptgs2* Expression in Esr2-PgrKO Granulosa Cells

(A) UMAP clustering identified 18 different cell clusters in the mouse ovary. Dotted lines show major cell populations that were identified by the expression of marker genes (red characters).

(B) Differentially expressed genes (DEGs) of ovulatory mural granulosa cells (Ov-mural-1 and −2), ovulatory cumulus cells (Ov-cumulus), and immune cells (Immune) were marked in scatterplots. Red circles indicate *Ptgs2*, which is upregulated in Esr2-PgrKO (KO) compared to WT. Blue circles indicate inflammation-related genes that are upregulated in KO compared to WT.

(C) Violin plots show the expression levels of *Ptgs2* and *S100a6* in ovarian cell clusters. Expression of *Ptgs2* and *S100a6* are increased and decreased in ovulatory granulosa cells (clusters 0, 3, and 4), respectively.

(D) UMAP plot in the solid box shows sub-clusters of granulosa cells. Feature plots for *Pgr* and *Ptgs2* in WT and KO show the exclusive expression pattern of *Pgr* and *Ptgs2* mRNA in granulosa cells.

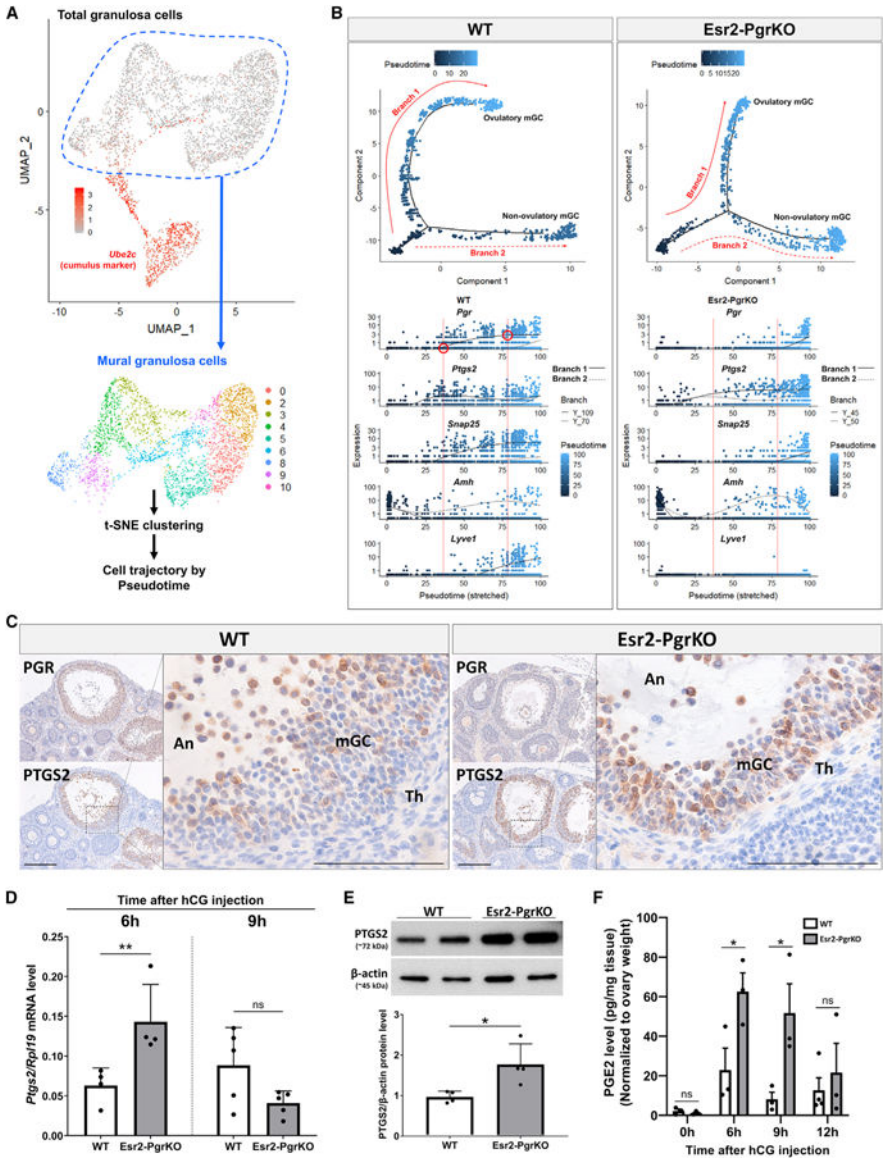

Figure 3. Elevated *Ptgs2* Expression in Granulosa Cells of Esr2-PgrKO Mice

(A) UMAP clustering shows the granulosa cells. Ube2c-negative mural granulosa cells (dotted area) were isolated from the total granulosa cell population and used for t-SNE clustering and cell trajectory.

(B) Cell trajectories by pseudotime in mural granulosa cells of WT and Esr2-PgrKO show two different states (Branch-1 and −2) of mural granulosa cells at the end of pseudotime. Changes in expression of *Amh*, *Lyve1*, *Pgr*, *Ptgs2*, and *Snap25* in Branch-1 and −2 are shown by pseudotime plot. Red circles in the pseudotime plot indicate when the *Pgr* gene begins to be expressed and when it reaches its highest expression level, respectively. Ovulatory granulosa cells (cells in Branch-1) express *Pgr*, whereas non-ovulatory granulosa cells (cells in Branch-2) do not express *Pgr* until the Pgr expression level in Branch-1 reaches the highest level.

(C) Localization of PGR and PTGS2 protein in preovulatory follicles at 9 h after hCG injection. An, Antrum; mGC, mural granulosa cells; Th, theca cells (scale bar, 0.1 mm).
(D) *Ptgs2* mRNA level in isolated granulosa cells from WT and Esr2-PgrKO ovaries at 6 h and 9 h after hCG injection. Error bars, SD (n = 4); **p<0.01 (Student's t test).
(E) Ovarian PTGS2 protein level in WT and Esr2-PgrKO mice at 9 h after hCG injection. Error bars, SD (n = 4); *p < 0.05 (Student's t test).
(F) PGE2 concentration in WT and Esr2-PgrKO ovaries at 0, 6, 9, and 12 h after hCG injection. Error bars, SD (n = 3–4); *p < 0.05 (Student's t test).

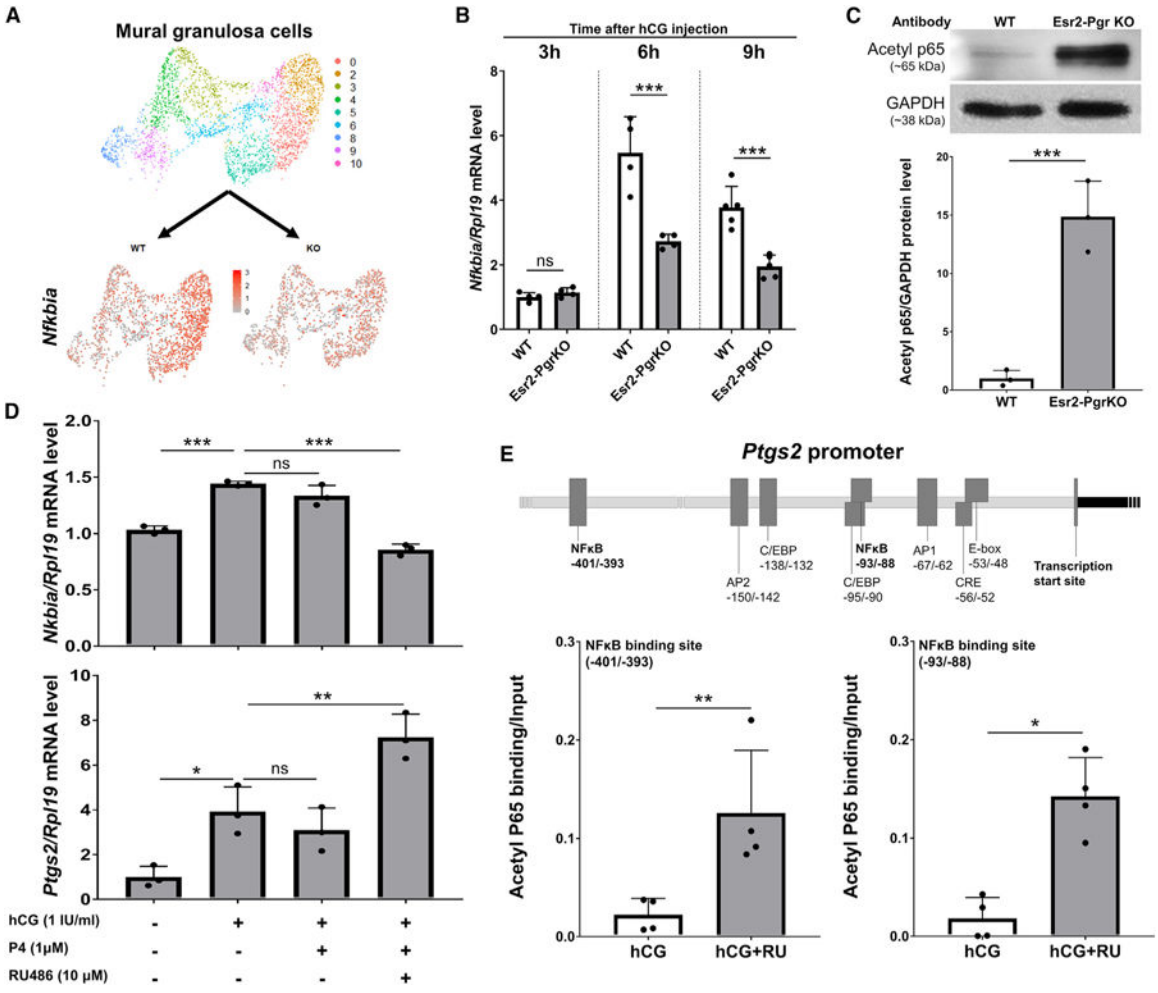

Figure 4. PGR Suppresses *Ptgs2* mRNA Expression in Granulosa Cells by NF-κB Inhibition

(A) Localization of *Nkbia*-expressing cells in UMAP plot for mural granulosa cells. *Nfkbia* mRNA expression intensity is marked with a gray-red color scale in dots.

(B) Changes in *Nfkbia* mRNA in isolated granulosa cells in superovulated WT and Esr2-PgrKO. Granulosa cells were isolated from the ovary at 3 h, 6 h, and 9 h after hCG injection and analyzed by real-time PCR. Error bars, SD (n = 4); ***p < 0.001 (Student's t test).

(C) Quantification of acetyl-p65 protein in granulosa cells of WT and Esr2-PgrKO at 3 h after hCG treatment. Error bars, SD (n = 3); ***p < 0.001 (Student's t test).

(D) Granulosa cells were isolated from the preovulatory ovary at 48 h after PMSG injection. Granulosa cells were cultured with or without hCG for 3 h and then treated with P4 (progesterone) alone or with RU486 for 3 h. *Nfkbia*, *Ptgs2*, and *Rpl19* mRNA levels were measured by real-time PCR using specific primers. Error bars, SD (n = 3); *p < 0.05, **p < 0.01, and ***p < 0.001 (ANOVA and Tukey's post hoc test).

(E) Known transcription binding sites in the promoter of the *Ptgs2* gene, including NF-κB binding sites. Graphs indicate the binding of acetyl-p65 to each NF-κB binding site of the *Ptgs2* promoter in lysates from granulosa cells under basal conditions and RU486-treated condition. Error bars, SD (n = 3); *p < 0.05 and **p < 0.01 (Student's t test).

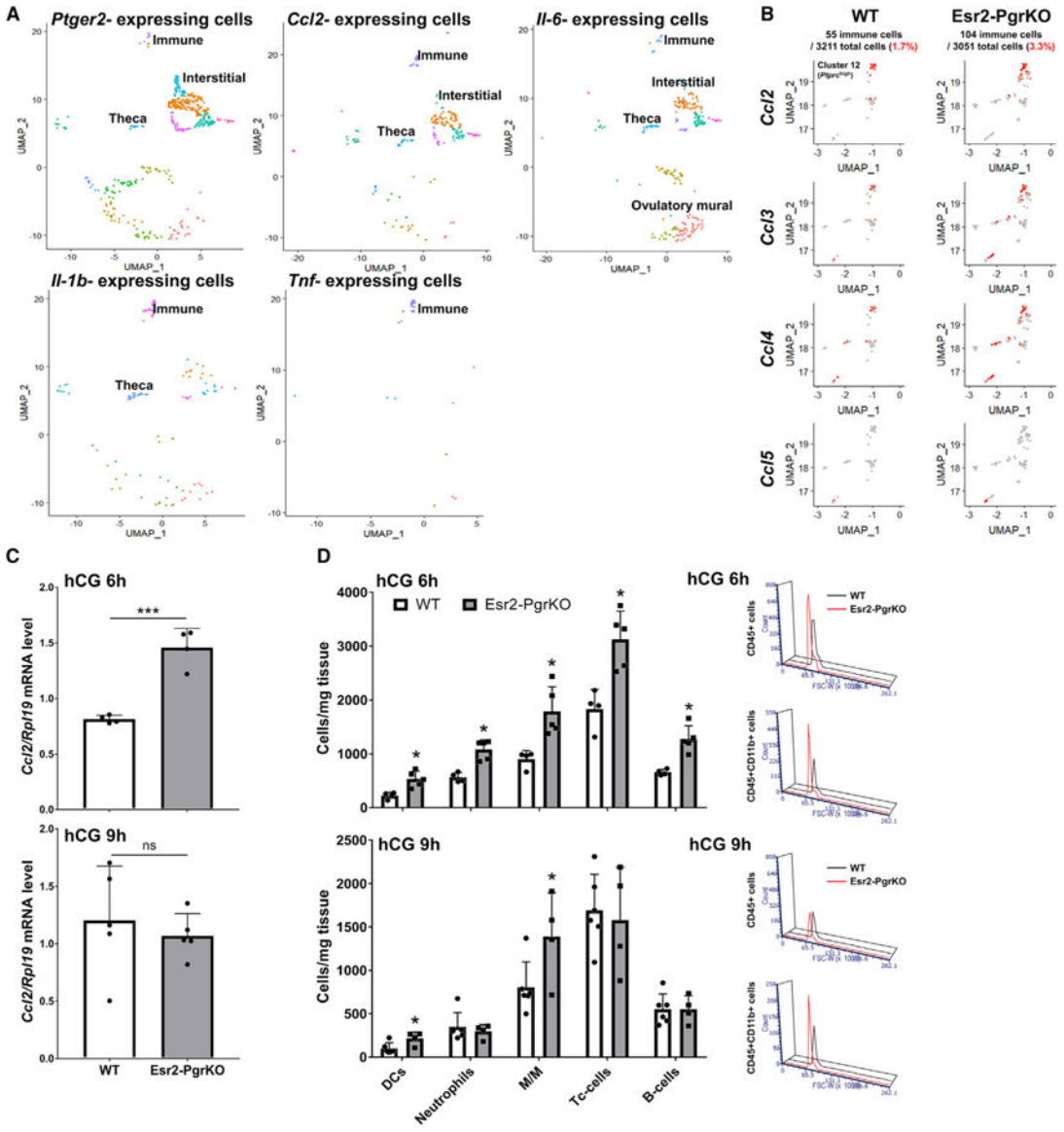

Figure 5. *Pgr* Ablation in Granulosa Cells Results in an Elevated Ovarian Immune Cell Population

(A) Expression of cytokines in *Ptger2*-expressing ovarian cells. *Ptger2*, *Ccl2*, and *Il6* are expressed in theca, interstitial, and immune cells in the ovary at hCG 6 h. *Il1b* is expressed in immune cells and theca cells. *Tnf* is expressed in only immune cells. Each dot indicates LogExp > 0.5 for each observed gene.

(B) UMAP plots for immune cell population (*Ptprc*-positive cells) show the expression and localization of chemokine genes, including *Ccl2*, *−3*, *−4*, and *−5*. Red dots in the plot indicate relatively higher gene expression levels.

(C) *Ccl2* mRNA levels in GCs of WT and Esr2-PgrKO ovaries at 6 h and 9 h after hCG injection. Error bars, SD (n = 4–5); ***p<0.001 (Student's t test).

(D) Leukocyte population in WT and Esr2-PgrKO ovaries at 6 h and 9 h after hCG injection. Error bars, SD (n = 5); *p < 0.05 (Student's t test). DCs, dendritic cells; M/M, monocytes and macrophages.

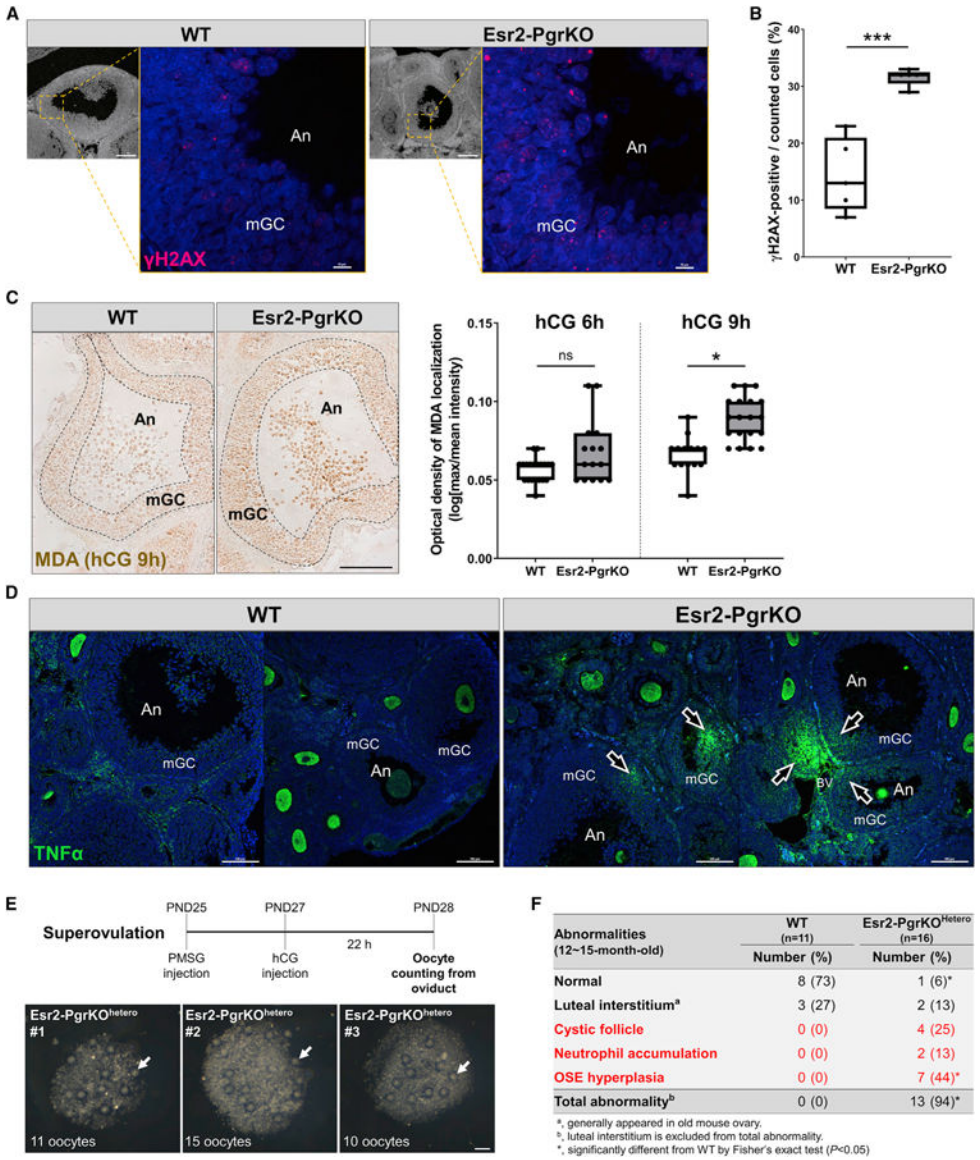

Abnormalities (12~15-month-old)	WT (n=11) Number (%)	Esr2-PgrKO^{Hetero} (n=16) Number (%)
Normal	8 (73)	1 (6)*
Luteal interstitium[a]	3 (27)	2 (13)
Cystic follicle	0 (0)	4 (25)
Neutrophil accumulation	0 (0)	2 (13)
OSE hyperplasia	0 (0)	7 (44)*
Total abnormality[b]	0 (0)	13 (94)*

[a], generally appeared in old mouse ovary.
[b], luteal interstitium is excluded from total abnormality.
*, significantly different from WT by Fisher's exact test (P<0.05)

Figure 6. Ablation of *Pgr* Causes Increased Oxidative Stress and Inflammatory Damage in the Ovary

Mice were injected with hCG following PMSG injection (48 h). Ovaries were collected from WT and Esr2-PgrKO mice at 6 h after hCG injection and subjected to immunohistochemistry or immunofluorescent examination.

(A) Immune-localization of γH2AX (red) in antral follicles of WT and Esr2-PgrKO ovaries (scale bars in bottom magnification, 0.1 mm; scale bars in top magnification, 10 μm).

(B) Quantitative analysis of γH2AX-positive cells in mural granulosa cell layer of antral follicles. Five different antral follicles in WT and Esr2-PgrKO were subjected to quantitative analysis. Error bars, SD (n = 5); ***p < 0.001 (Student's t test).

(C) Immune-localization of malondialdehyde (brown) in ovarian follicles of WT and Esr2-PgrKO. Optical intensity of the brown channel was quantified and compared between WT and Esr2-PgrKO at hCG 6 and 9 h (scale bar, 50 μm). Error bars, SD (n = 12–20); *p < 0.01 (Student's t test).

(D) Immune-localization of TNFα (green) in WT and Esr2-PgrKO ovaries. Arrows indicate TNFα invasion into the follicles. An, Antrum; mGC, mural granulosa cells (scale bars, 100 μm).

(E) The number of ovulated oocytes was counted in $Pgr^{flox/wt}Esr2^{iCre/wt}$ after inducing of superovulation. Arrows indicate the ovulated oocytes from a single ovary (scale bars, 100 μm).

(F) Frequency of occurrence of major abnormalities in WT and Esr2-$PgrKO^{hetero}$ ovaries at the age of 12–15 months after birth.

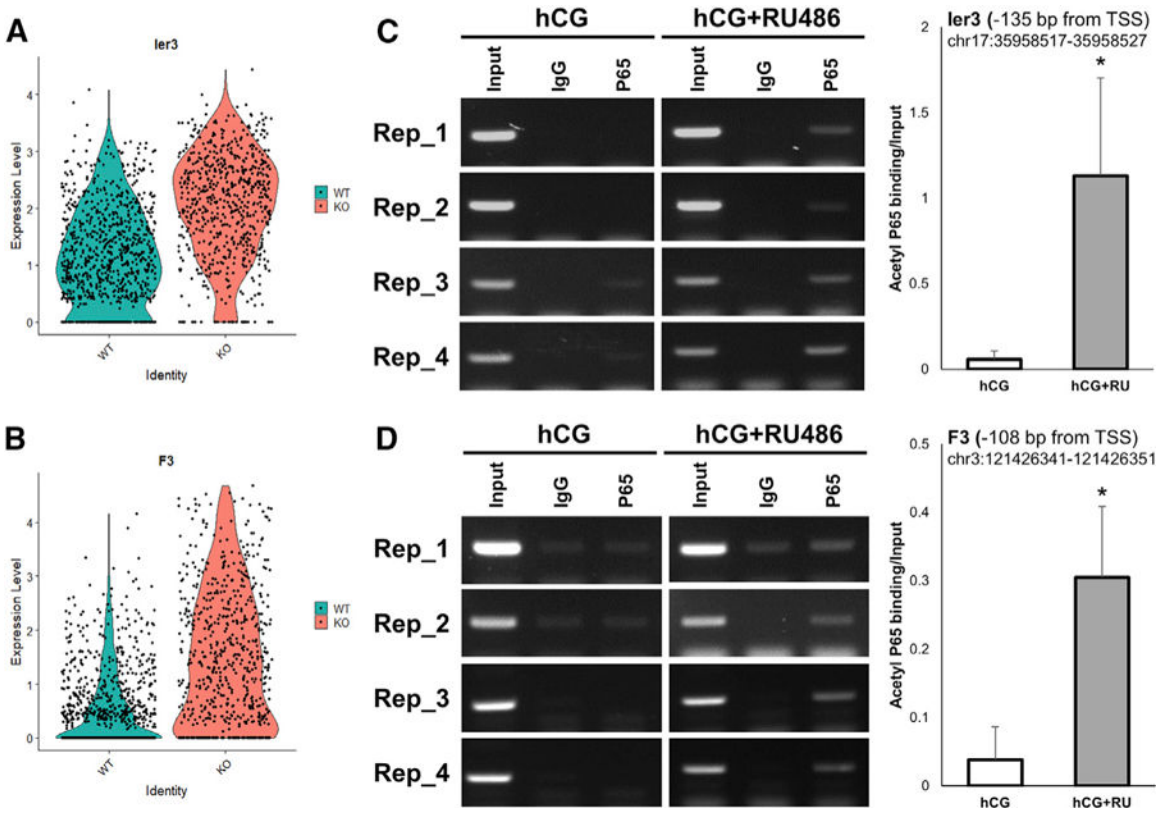

Figure 7. Increased P65 Binding on Ier3 and F3 Gene Promoter by Inhibition of PGR Activity

(A) Comparison of *Ier3* expression level between WT and Esr2-PgrKO.

(B) Comparison of *F3* expression level between WT and Esr2-PgrKO.

(C) Binding of acetyl-p65 to predicted NF-κB binding site of the *Ier3* promoter in lysates from granulosa cells under basal conditions and RU486-treated condition. Error bars, SD (n = 4); *p < 0.05 (Student's t test).

(D) Binding of acetyl-p65 to predicted NF-κB binding site of the *F3* promoter in lysates from granulosa cells under basal conditions and RU486-treated condition. Error bars, SD (n = 4); *p < 0.05 (Student's t test).